JOURNAL OF Materials CHEMISTRY

Design and synthesis of light-harvesting rods for intrinsic rectification of the migration of excited-state energy and ground-state holes†

Robert S. Loewe,[a] Robin K. Lammi,[b] James R. Diers,[c] Christine Kirmaier,[b] David F. Bocian,*[c] Dewey Holten*[b] and Jonathan S. Lindsey*[a]

[a]*Department of Chemistry, North Carolina State University, Raleigh, North Carolina, 27695-8204, USA*
[b]*Department of Chemistry, Washington University, St. Louis, Missouri, 63130-4889, USA*
[c]*Department of Chemistry, University of California, Riverside, California, 92521-0403, USA*

Received 8th September 2001, Accepted 20th January 2002
First published as an Advance Article on the web 18th March 2002

We present the design of molecular materials for ultimate use in solid-state solar cells. The molecular materials are semi-rigid oligomeric rods of defined length with metalloporphyrins in the backbone and a carboxy group at one end for attachment to a surface. The rods are designed to absorb visible light, and then undergo excited-state energy transfer and ground-state hole transfer in opposite directions along the length of the rod. The rational synthesis of the multiporphyrin arrays relies on joining porphyrin building blocks in an efficient and controlled manner. Several porphyrin building blocks have been synthesized that bear bromophenyl, iodophenyl, trimethylsilylethynylphenyl and/or ethynylphenyl substituents for use in a copper-free Sonogashira reaction using $Pd_2(dba)_3$ and P(*o*-tol)$_3$. Competition experiments performed on equimolar quantities of an iodo-porphyrin and a bromo-porphyrin with an ethynyl-porphyrin show iodo + ethyne coupling with a low amount (35 °C) or undetectable amount (22 °C) of bromo + ethyne coupling. Efficient coupling of bromo-porphyrins with ethynyl-porphyrins was achieved using the same copper-free Sonogashira reaction conditions at higher temperature (50 °C or 80 °C). These findings allow successive coupling reactions to be achieved using substrates bearing iodo and bromo synthetic handles. Thus, a porphyrin-based tetrad (or pentad) was synthesized with a final convergent coupling of a bromo-substituted dyad (or triad) and an ethynyl-substituted dyad. A porphyrin triad was prepared by sequential iodo + ethyne coupling reactions. The triad, tetrad, and pentad each are comprised of a terminal magnesium porphyrin bearing one carboxy group (for surface attachment) and two pentafluorophenyl groups; the remaining porphyrins in each array are present as the zinc chelate. Electrochemical characterization of benchmark porphyrins indicates the presence of the desired electrochemical gradient for hole hopping in the arrays. Static absorption data indicate that the arrays are weakly coupled, while static fluorescence data indicate that the excited-state energy flows in high yield to the terminal magnesium porphyrin. Time-resolved spectroscopic analysis leads to rate constants in THF of $(9\ ps)^{-1}$, $(15\ ps)^{-1}$, and $(30\ ps)^{-1}$ for ZnMg dyad **20**, Zn_2Mg triad **13**, and Zn_3Mg tetrad **15**, respectively, and quantum efficiencies $\geqslant$99% for energy flow to the magnesium porphyrin in each case. These design and synthesis strategies should be useful for the construction of materials for molecular-based solar cells.

Introduction

Porphyrinic pigments lie at the heart of the photosynthetic conversion of light into chemical energy.[1] Photosynthetic organisms employ a light-harvesting antenna complex comprised of numerous pigments coupled to a reaction center for energy transduction. Absorption of light by a pigment in the antenna is followed by rapid singlet excited-state energy migration among the antenna chromophores until the energy reaches the lowest energy site, the special pair of porphyrinic pigments in the reaction center. Vectorial excited-state electron transfer then occurs, with the electron moving along a chain of porphyrinic and other cofactors in the reaction center toward one side of the membrane. The hole remaining on the special pair migrates in the opposite direction toward the other membrane surface and out of the reaction center, thereby generating a transmembrane potential. In bacterial systems, hole transport is mediated by a series of iron porphyrins.[2] Thus, four major functions performed by porphyrinic pigments underlie photosynthetic function: light absorption, excited-state energy migration, excited-state electron transfer, and ground-state hole/electron migration. The efficiency of these combined processes stems from the overall design, the inherent optical/electronic properties of the pigments, and the 3-dimensional organization of all components.

Attempts to prepare molecular-based solar cells have generally employed molecules in conjunction with semiconductors. Three generic designs have been investigated: (I) a monolayer of pigment bound to a semiconductor surface; (II) a thin film of pigment deposited on a semiconductor surface; and (III) a monolayer of pigment bound to a mesoporous semiconductor surface. The absorption of light by the pigment results in electron injection into the semiconductor, yielding a charge-separated state. The hole residing on the pigment is then transferred (typically by a diffusive redox-active agent in a liquid) to the counter electrode, thereby completing the circuit. Achieving high efficiency in solar-energy conversion requires absorption of most of the incident light across the solar

†Electronic supplementary information (ESI) available: ^1H and ^{13}C NMR spectra for all new porphyrin precursors; ^1H NMR and LD-MS spectra for all new porphyrins and porphyrin arrays (LD-MS only for deprotected arrays **12′** and **14′**, and pentad **18**); analytical SEC data for all porphyrin arrays. See http://www.rsc.org/suppdata/jm/b1/b108168c/

 DOI: 10.1039/b108168c

spectrum, a high quantum yield of electron injection, a low quantum yield of charge recombination at the electrode surface, efficient electron transport in the semiconductor to the external circuit, and efficient transport of the hole to the counterelectrode. The three designs have a number of limitations. In design I, a monolayer of dye typically absorbs only a tiny fraction of the incident light. In design II, a thin film can absorb much of the incident light but the resulting excited-state energy may not reach the semiconductor surface, or the hole generated upon electron injection at the semiconductor may be trapped in the thin film and not reach the counter-electrode. In design III, although the dye is employed as a monolayer on the semiconductor surface, the mesoporous nature of the semiconductor material ensures high absorption of light. However, the mesoporous structure provides many opportunities for electron-hole recombination. The efficiencies of these solar cells range from $<1\%$ (case I) to a few percent (case II) to $\sim 10\%$ (case III).[3]

We are working toward a molecular-based solar cell that employs molecules in conjunction with semiconductors in a manner inspired by the design of natural photosynthetic systems. The molecular materials are light-harvesting rods that can be sandwiched between a semiconductor (anode) and a counterelectrode (cathode). The rod is a backbone oligomer comprised of porphyrinic pigments joined in a covalent manner. Absorption of light by one of the pigments yields the singlet excited state, which migrates from pigment to pigment along the backbone until reaching the lowest energy chromophore, the pigment directly attached to the semiconductor. This last pigment constitutes the electron-injection unit and undergoes excited-state electron transfer, injecting an electron into the semiconductor. The hole residing on the electron-injection unit then migrates among pigments in the light-harvesting rod until the counterelectrode is reached, thereby completing the circuit and regenerating the rod for another photocycle.

A key feature of the molecular design is the ability to cause excited-state energy and ground-state holes to migrate in opposite directions along a given light-harvesting rod. Such intrinsic rectification is possible because the physics of the two processes are fundamentally different, as shown in Fig. 1. Energy transfer is an excited-state process. Energy transfer among neighboring pigments occurs reversibly with isoenergetic pigments and from donor to acceptor when the excited-state energy (ΔE) of the acceptor is lower than that of the donor. Thus, excited-state energy flows along a rod from pigment i + 1 to pigment i with excited-state energies such that

$$\Delta E_{(i)} < \Delta E_{(i+1)} \quad (1)$$

The migration of holes is a ground-state process and the direction of transfer depends on the value of the electrochemical midpoint potential ($E_{1/2}$) for the one-electron oxidation of each pigment in the rod. Ground-state hole transfer among neighboring pigments occurs reversibly with isoenergetic pigments, and irreversibly from (oxidized) pigment i to (non-oxidized) pigment i + 1 when the electrochemical potentials are such that

$$E_{1/2(i)} > E_{1/2(i+1)} \quad (2)$$

Thus, a light-harvesting rod comprised of a chain of pigments that satisfies eqns. (1) and (2) should afford intrinsic rectification in the migration of excited-state energy and ground-state holes. This is illustrated pictorially in Fig. 1. The excited energy flows along the rod toward the anode while hole migration occurs from the pigment (electron-injection unit) adjacent to the anode back toward the cathode.

In summary, this design provides the same four functions as are present in natural photosynthetic systems: absorption of light, transfer of excited-state energy to a specific site, vectorial excited-state electron transfer, and vectorial ground-state hole migration. It is noteworthy that this design does not require a diffusive charge carrier in a liquid as do many molecular-based solar cells constructed to date. Because the rods need only be long enough to provide efficient absorption of light (anticipated to be less than 50 porphyrinic pigments), the active medium in the solar cell is expected to have a thickness of less than 100 nm. Accordingly, this design should afford an ultrathin solid-state cell.

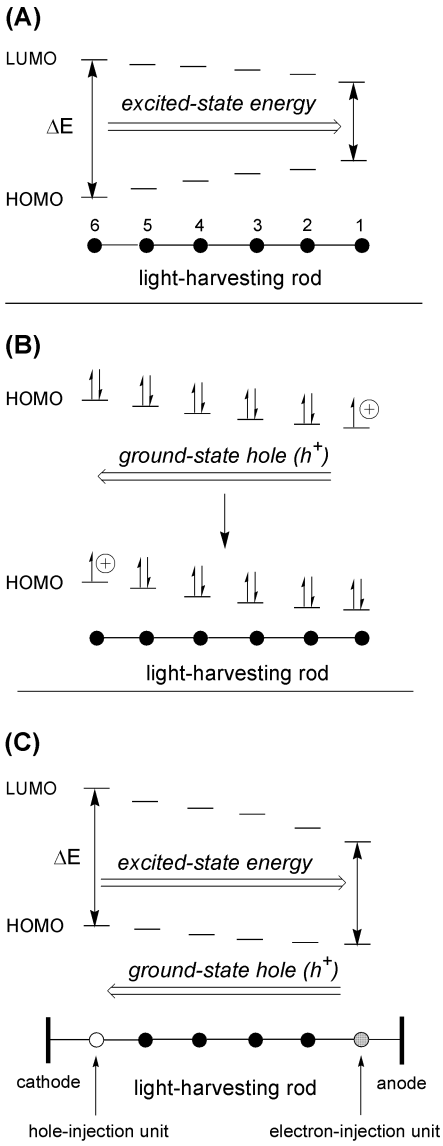

Fig. 1 Molecular physics considerations for designing light-harvesting rods. (A) The energy of the excited-state (ΔE) is given by the difference between the energies of the highest occupied molecular orbital (HOMO) and the lowest unoccupied molecular orbital (LUMO). Energy migration occurs from a pigment with large ΔE to a pigment with smaller ΔE. (B) The energy level of the ground-state hole is given by the electrochemical potential ($E_{1/2}$) for the one-electron oxidation, which depends only on the energy of the HOMO. Hole hopping occurs from a pigment with high potential to a pigment with low potential. (C) A light-harvesting rod composed of pigments with appropriate energy levels supports the flow of excited-state energy and ground-state holes in opposite directions (*i.e.*, intrinsic rectification).

We have shown that excited-state energy transfer occurs rapidly and efficiently in multiporphyrin arrays in which metalloporphyrins and/or free base porphyrins are joined *via* diphenylethyne[4,5] or *p*-phenylene linkers.[6] We have also shown that ground-state hole migration is facile among isoenergetic porphyrins in the same types of multiporphyrin arrays.[7,8] Furthermore, both processes can be tuned by design of the porphyrin components (which basically retain their inherent

photophysical/electronic characteristics when joined *via* diphenylethyne or *p*-phenylene linkers).[9] In pioneering studies of synthetic molecules designed for photoinduced charge-separation processes by Gust, Moore and Moore[10] and by Wasielewski,[11] hole migration (*via* a charge-shift reaction) away from the donor–acceptor pair and toward a redox-active component at less positive potential was found to provide a means of stabilizing the charge-separated state. The molecules in these early studies generally were comprised of carotenoid–porphyrin–quinone[10] or aniline–porphyrin–quinone[11] species, while more recent systems that undergo such a charge-shift reaction have included additional features such as (1) two porphyrins,[12] (2) arene–imides[13] or buckyballs[14] as electron acceptors in conjunction with multiple porphyrins, or (3) aniline–monoimide–diimide triads without any porphyrins.[15] Taken together, these data augur well for the design of molecules that support the intrinsic rectification of the migration of excited-state energy and ground-state holes along the length of a linear rod as described in eqns. (1) and (2). While the design appears robust, the synthesis of such rods requires the development of new synthetic strategies.

In this paper, we first describe the design strategy for constructing linear rods comprised of 3–5 porphyrins for intrinsic rectification of the migration of excited-state energy and ground-state holes. We then present the synthesis of porphyrin building blocks for construction of the linear rods. The porphyrins in the arrays are joined *via* diphenylethyne linkers, which are constructed in Pd-mediated coupling reactions of the porphyrin building blocks. Most prior syntheses of linear multiporphyrin arrays have employed divergent iterative coupling of iodo and ethynyl substituted porphyrin building blocks. To achieve convergence in the synthesis of the arrays, we performed a study of successive iodo + ethyne and bromo + ethyne coupling reactions with suitable porphyrin building blocks. The conditions identified for such successive couplings enabled the convergent synthesis of light-harvesting rods consisting of 4 or 5 porphyrins. We conclude with the characterization of the intrinsic properties of the components and arrays using electrochemical, static absorption and fluorescence, and time-resolved absorption techniques.

Results and discussion

1 Molecular design

Designs for achieving the directed flow of energy in an array of porphyrins have frequently employed a metalloporphyrin as the donor and a free base (Fb) porphyrin as the acceptor. However, the cation radicals of Fb porphyrins are generally unstable, making these molecules poor choices to serve as the simultaneous energy recipient (from the rod) and electron injector (to the electrode). On the other hand, the cation radicals of many metalloporphyrins are quite stable.[16] The lowest energy absorption of a magnesium (Mg) porphyrin typically occurs ~10 nm to longer wavelength (0.035 eV to lower energy) than that of the corresponding zinc (Zn) porphyrin, enabling a Mg porphyrin to serve as the energy acceptor with a Zn porphyrin (or multiple Zn porphyrins) as the energy donor. On the other hand, a Mg porphyrin generally exhibits an $E_{1/2}$ value that is ~150 mV less positive than that of the corresponding Zn porphyrin (*i.e.*, the former is more easily oxidized).[17,18] Thus, hole migration cannot occur from a Mg porphyrin to a Zn porphyrin if the porphyrin macrocycles are identical. However, the $E_{1/2}$ values of porphyrins can be tuned by incorporating electron-deficient or electron-rich substituents at the perimeter of the macrocycle with little change on the position of the long-wavelength absorption band.[18] Thus, the design we sought incorporated an electron-deficient Mg porphyrin as the electron-injection unit at the terminus of the rod. For attachment to a metal-oxide semiconductor, a carboxylic acid group was required on the Mg porphyrin. Zn porphyrins of less positive $E_{1/2}$ values (increasing electron-richness) could then be incorporated in the rod with increasing distance from the Mg porphyrin to facilitate hole migration away from the electron-injection point and thus toward the counter electrode.

To identify suitable peripheral substituents for Zn or Mg porphyrins, an initial survey was performed on a small family of metalloporphyrins. The Fb porphyrins had been prepared previously and were metalated under standard conditions. The results are shown in Table 1. The Mg porphyrin must have a more positive $E_{1/2}$ value and a lower energy long-wavelength absorption band than any of the Zn porphyrins in the array. Considering zinc tetraphenylporphyrin (ZnTPP, **Zn-1a**) or zinc tetramesitylporphyrin (ZnTMP, **Zn-1b**) as the least electron-rich of any Zn porphyrin that might be employed, a Mg porphyrin with two pentafluorophenyl groups (**Mg-1e**) satisfies both criteria whereas one pentafluorophenyl group yields a Mg porphyrin that is insufficiently electron-deficient (**Mg-1d**). We investigated the use of trifluoromethyl groups, which cause a large positive shift in the $E_{1/2}$ value (*e.g.*, **Zn-1f**), but were unable to obtain the magnesium chelate. The introduction of two *p*-methoxy groups to ZnTPP (*i.e.*, **Zn-1c**) shifts the $E_{1/2}$ value to less positive values by ~30 mV. With these results in hand, we considered satisfactory designs to incorporate the following sequence of pigments: a TMP-type Zn porphyrin

Table 1 Q(0,0) Absorption maxima and electrochemical data for representative metalloporphyrins

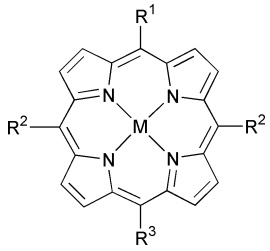

Porphyrin	R^1	R^2	R^3	M	λ_{abs} Q(0,0)[a]	$E_{1/2}$/mV[b]
Zn-1a	Phenyl	Phenyl	Phenyl	Zn	590	0.56
Zn-1b	Mesityl	Mesityl	Mesityl	Zn	590	0.51
Zn-1c	*p*-Methoxyphenyl	Phenyl	*p*-Methoxyphenyl	Zn	592	0.53
Mg-1d	Pentafluorophenyl	*p*-Tolyl	Phenyl	Mg	604	0.50
Mg-1e	Pentafluorophenyl	Phenyl	Pentafluorophenyl	Mg	604	0.66
Zn-1f	Trifluoromethyl	Mesityl	Trifluoromethyl	Zn	588	0.87

[a]In toluene. [b]$E_{1/2}$ *vs.* Ag/Ag^+ in CH_2Cl_2 containing 0.1 M Bu_4NPF_6; $E_{1/2}$ of $FeCp_2/FeCp_2^+$ is 0.19 V; scan rate 0.1 V s^{-1}.

bearing two alkoxy groups, a TMP-type Zn porphyrin bearing one alkoxy group, a TMP-type Zn porphyrin without other substituents, and a Mg porphyrin bearing two pentafluorophenyl groups. The presence of a *p*-carboxy group on the Mg porphyrin should not adversely affect the desired property of the array, only shifting the $E_{1/2}$ to a more positive value compared with the benchmark compound **Mg-1e**.

Two other points that bear on design are noteworthy. First, domains of adjacent isoenergetic pigments can be employed, affording reversible transfer processes. Second, we have shown that excited-state energy migration and ground-state hole-hopping can occur rapidly between non-nearest-neighbor porphyrins, utilizing the intervening porphyrin and linkers as superexchange mediators.[7–9,19] Thus, the presence of one pigment (or a small domain of pigments) in a rod with slightly inappropriate energy/$E_{1/2}$ characteristics will slow, but not cause termination of, the flow of excited-state energy or ground-state holes.

2 Synthesis

Porphyrin building blocks. Many of the porphyrin building blocks employed in this study were synthesized following a method for preparing porphyrins bearing up to four different meso substituents.[20] The starting point for such porphyrins begins with the synthesis of 5-substituted dipyrromethanes. Thus, the one-flask reaction of an aldehyde and excess pyrrole at room temperature afforded dipyrromethanes **2a–g** (Scheme 1).[21] Dipyrromethanes **2a–e** were purified by distillation followed by recrystallization while dipyrromethanes **2f,g** were purified by column chromatography followed by recrystallization. These dipyrromethanes are key precursors to the requisite porphyrin building blocks.

Monoacyl dipyrromethane **3**[20] was treated with EtMgBr followed by an acid chloride (**4a–c**) affording the corresponding diacyldipyrromethane (**5a–c**) in good yield (Scheme 2). These compounds are important precursors in the synthesis of *trans*-AB_2C- and ABCD-porphyrin building blocks.

The dipyrromethanes **2b,d,e** were treated with EtMgBr and pentafluorobenzoyl chloride, affording diacyldipyrromethanes **5d–f** (Scheme 3). Compounds **5d,e** serve as direct precursors to *trans*-AB_2C-porphyrins while compound **5f** is employed as a building block in the synthesis of an A_3B-porphyrin.

The target porphyrin building blocks were prepared by reducing the appropriate diacyldipyrromethane (**5a–f**) to the corresponding dipyrromethane-dicarbinol using excess $NaBH_4$.[20] The dipyrromethane-dicarbinol was then condensed with the

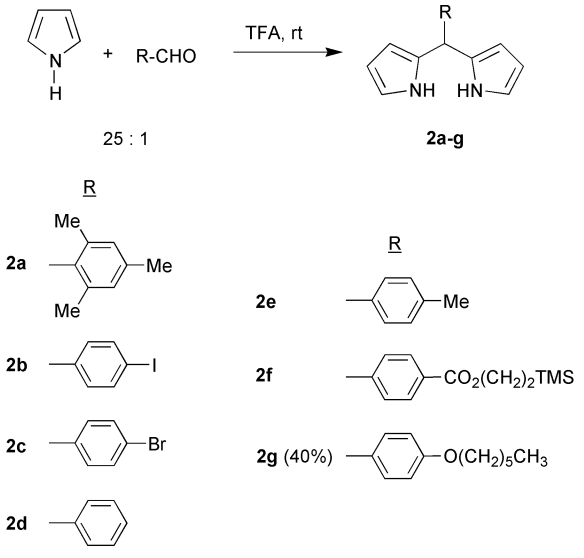

Scheme 1

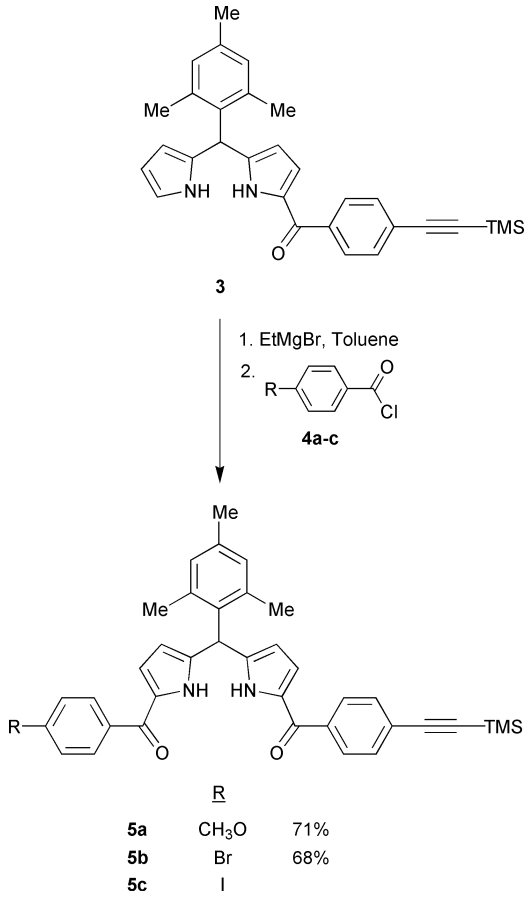

Scheme 2

appropriate dipyrromethane (**2a–g**) under non-scrambling conditions (30 mM trifluoroacetic acid (TFA) in CH_3CN at room temperature) for a few minutes, followed by the addition of 2,3-dichloro-5,6-dicyano-1,4-benzoquinone (DDQ) to achieve

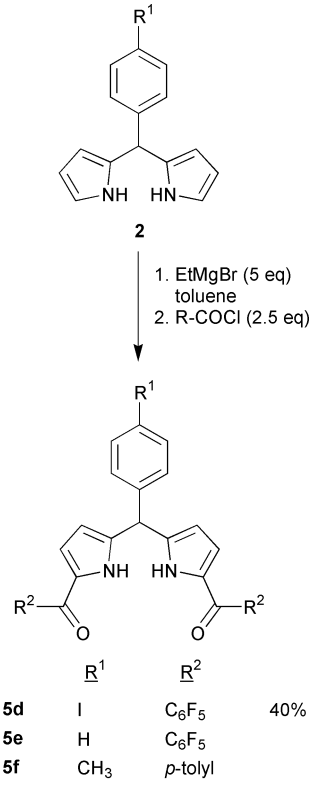

Scheme 3

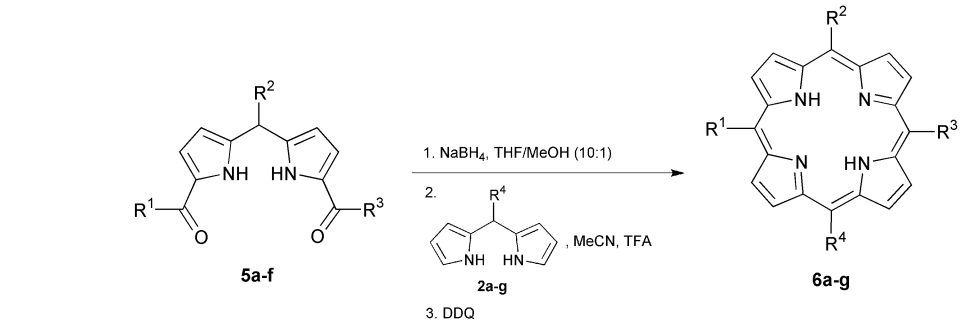

R^1	R^2	R^3	R^4	Product	Yield
CH_3O	3,4,5-trimethylphenyl	TMS	$CH_3(CH_2)_5O$	**6a**	22%
I	3,4,5-trimethylphenyl	TMS	$CH_3(CH_2)_5O$	**6b**	22%
Br	3,4,5-trimethylphenyl	TMS	3,4,5-trimethylphenyl	**6c**	26%
I	3,4,5-trimethylphenyl	TMS	3,4,5-trimethylphenyl	**6d**	22%
2,3,5,6-tetrafluorophenyl	I	2,3,5,6-tetrafluorophenyl	TMS-ethyl-oxycarbonylphenyl	**6e**	18%
2,3,5,6-tetrafluorophenyl	phenyl	2,3,5,6-tetrafluorophenyl	TMS-ethyl-oxycarbonylphenyl	**6f**	19%
Me	Me	Me	Br	**6g**	25%

Scheme 4

oxidation (Scheme 4).[20] Following this procedure, ABCD-porphyrins **6a,b**, *trans*-AB_2C-porphyrins **6c–f**, and A_3B-porphyrin **6g** were prepared in yields ranging from 18 to 26%. In each case, analysis of the crude reaction mixture by laser desorption mass spectrometry (LD-MS) showed no detectable formation of new porphyrins derived from acidolysis and undesired recombination (*i.e.* scrambling). The porphyrins were purified in the following manner: (1) filtration of the crude reaction mixture through alumina to remove quinone species, (2) removal of solvent under reduced pressure, (3) one silica gel chromatography procedure to remove non-porphyrinic pigments, and (4) sonication of the porphyrin product suspended in methanol followed by filtration to remove trace amounts of soluble impurities.

Porphyrins **6a–d** and **6g** were metalated using $Zn(OAc)_2 \cdot 2H_2O$ in $CHCl_3$ to afford the zinc chelates **Zn-6a–d** and **Zn-6g** in yields ranging from 75 to 94%. Porphyrins **6e,f** were metalated using $MgBr_2 \cdot O(Et)_2$ and triethylamine in CH_2Cl_2 to afford the magnesium chelates **Mg-6e,f**.[22] Porphyrin **6g** was also metalated using MgI_2 and *N,N*-diisopropylethylamine in CH_2Cl_2 to give the magnesium chelate **Mg-6g** in 81% yield. Removal of the trimethylsilyl (TMS) protecting group of porphyrin **Zn-6a** or **Zn-6c** was achieved using tetra-*n*-butylammonium fluoride (TBAF) in THF–$CHCl_3$ (2 : 1) to afford porphyrin **Zn-6a′** or **Zn-6c′** in 96% or 77% yield, respectively. Porphyrins **Mg-6h**, **Mg-6i′**, and **Zn-6i′** were each obtained from a mixed-aldehyde condensation followed by metal insertion and subsequent deprotection where required. These porphyrin building blocks were employed in the cross-coupling experiments and array syntheses described below (see Schemes 5 and 6).

Investigation of successive ethyne + halo coupling as a means of convergence. The design of the light-harvesting rods requires control over the composition of each porphyrin unit in the rod. Thus, a stepwise synthetic method is suggested. The synthesis of diphenylethyne-linked multiporphyrin arrays *via* the Sonogashira reaction entails the palladium-catalyzed cross-coupling of porphyrins bearing iodophenyl and ethynylphenyl substituents.[23–25] Several routes are outlined in Fig. 2. The distinctions among these methods include the number of porphyrin building blocks employed, the number of coupling steps, the severity of the conditions, and the control afforded over the composition of the target array.

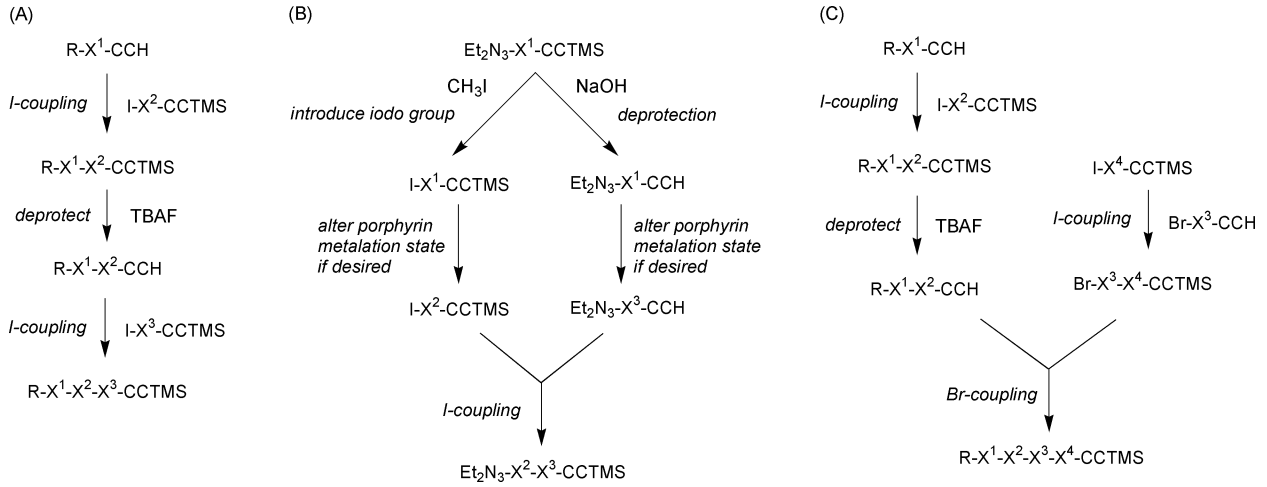

Fig. 2 Synthetic routes for the preparation of multiporphyrin arrays. "X" refers to a porphyrinic component. (A) Iterative divergent coupling yielding a porphyrin triad. (B) Iterative divergent–convergent coupling employing the use of the *N,N*-diethyltriazene moiety as a latent iodo group (transformed upon treatment with methyl iodide at 100 °C), yielding a porphyrin dyad. This cycle can be repeated to construct longer arrays. (C) Iterative divergent–convergent coupling employing successive iodo + ethyne and bromo + ethyne reactions, yielding a porphyrin tetrad.

The divergent, iterative coupling of an ethynyl-porphyrin and a porphyrin bearing an iodo group plus a trimethylsilyl-protected ethyne affords a porphyrin dyad (Fig. 2A). Cleavage of the trimethylsilyl group unveils the free ethyne and sets the stage for a second Pd-mediated coupling reaction with another bifunctional iodo/trimethylsilylethynyl porphyrin. This strategy works well for small arrays[26] but lacks the power of convergence needed to gain entry into larger arrays. One convergent approach, first demonstrated by Moore in the synthesis of oligomers of ethynylphenyl units[27] and extended by Gossauer to porphyrins,[28] employs a porphyrin building block bearing one *N,N*-diethyltriazene group and one trimethylsilylethyne group (Fig. 2B). One batch is reacted with methyl iodide, which results in replacement of the *N,N*-diethyltriazene group with the iodo group, forming the iodo/trimethylsilylethynyl porphyrin. The other batch is deprotected with base or fluoride, forming the *N,N*-diethyltriazene/ethynyl porphyrin. Each porphyrin can be demetalated and/or metalated as desired. The two porphyrins are then subjected to a standard Sonogashira reaction, yielding the ethyne linkage joining the dyad. Repetition of this cycle of divergent/convergent reactions (not shown) has been used to create a hexameric array of porphyrins.[28]

A complementary approach toward achieving convergence in the use of the Sonogashira reaction could be achieved by performing a selective iodo + ethyne coupling followed by a bromo + ethyne coupling (Fig. 2C). In this regard, several examples with small organic molecules have demonstrated selective coupling of the iodo functionality in the presence of the bromo functional group.[29] However, no previous attempts have been made to examine bromo-porphyrins in this capacity.

Chemoselectivity of iodo versus *bromo coupling.* To identify conditions for performing successive Sonogashira couplings, we first examined the selectivity of cross-coupling of an iodo-porphyrin and an ethynyl-porphyrin in the presence of a bromo-porphyrin. In this competition experiment, equimolar quantities of **Mg-6g**, **Mg-6h** and **Mg-6i′** were subjected to Sonogashira coupling conditions developed previously for the synthesis of multiporphyrin arrays (Scheme 5).[24,25] The progress of this reaction was monitored by analytical size-exclusion chromatography (SEC) and LD-MS. Tolyl and mesityl groups were employed in the bromo-porphyrin and iodo-porphyrin, respectively, to provide an adequate mass difference between dyads **7** and **8**, allowing for analysis by LD-MS (**7** has 1546 amu; **8** has 1464 amu). Dyad **7** is the product from the desired iodo + ethyne coupling reaction; dyad **8** is the product from unwanted bromo + ethyne coupling.

Upon reaction at 35 °C, analysis of both crude and purified samples by LD-MS showed a large mass envelope centered at m/z = 1546 corresponding to dyad **7**, as well as a small peak centered at m/z = 1464 corresponding to dyad **8** (Fig. 3A). These results indicate preferential but not exclusive selectivity for Sonogashira coupling with the iodo-porphyrin *versus* bromo-porphyrin. Upon reaction at room temperature (22 °C) instead of 35 °C, both the matrix-assisted laser desorption ionization mass spectrometry (MALDI-MS) using the matrix 1,4-bis(5-phenyloxazol-2-yl)benzene (POPOP) and LD-MS spectra of the crude and purified samples showed a very clean dyad mass region. Fig. 3B shows the MALDI-MS (POPOP) spectrum of the purified dyad fraction. No mass envelope corresponding to **8** could be detected. Thus, the lower reaction temperature reduces the amount of bromo + ethyne coupling to undetectable levels by MALDI-MS. However, the lower reaction temperature also slowed the rate of cross-coupling as evidenced by the analytical SEC data: after 2 h the percent conversion to dyad was nearly twice as high at 35 °C compared to 22 °C (63% *vs.* 34%).[30] Nevertheless, the absence of a detectable amount of bromo coupling products at the slightly lower reaction temperature makes this the preferred reaction condition.

Sonogashira coupling with bromo-porphyrins. The ability to perform successive Sonogashira couplings with iodo and bromo groups requires satisfactory conditions for bromo + ethyne coupling. In the first experiment, porphyrins **Zn-6g** and **Zn-6i′** were subjected to our standard Pd-coupling conditions with two modifications: (1) a 2 : 1 ratio of P(*o*-tol)$_3$: Pd was employed rather than the usual 4 : 1 ratio thereby generating a more active catalytic system, and (2) the reaction temperature was 80 °C (Scheme 6). Aliquots were removed and analyzed at 1 and 3 h by SEC and LD-MS, then the crude reaction mixture was purified according to established procedures.[25] The analytical SEC data showed no change in the amount of dyad formation at 1 h and 3 h (60% dyad after 1 h; 62% dyad after 3 h).[30] There was a significant amount of higher molecular weight material (HMWM) present at both timepoints (14% after 1 h; 17% after 3 h). The LD-MS data of purified **9** showed an intense peak centered at 1550 amu (Fig. 4). No observable peaks resulting from tolylation (1642 amu) or homocoupling (1512 amu) could be detected, indicating the cleanliness of this reaction.

A second experiment was performed with the following modifications: (1) the reaction was carried out at 50 °C, (2) a 4 : 1 ratio of P(*o*-tol)$_3$: Pd was employed, and (3) magnesium bromo-porphyrin **Mg-6g** was used in place of zinc bromo-porphyrin **Zn-6g** to test compatibility with the more

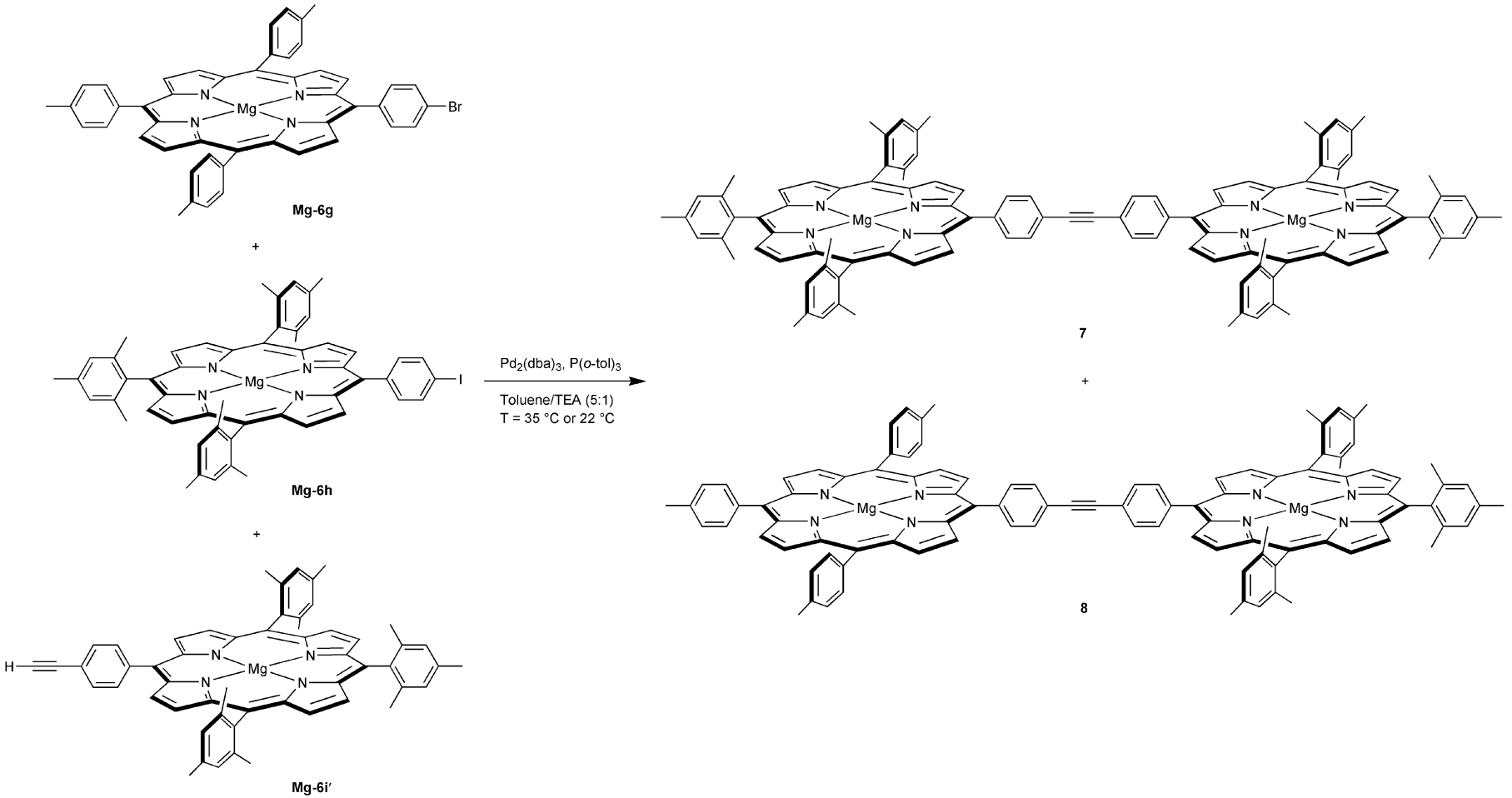

Scheme 5

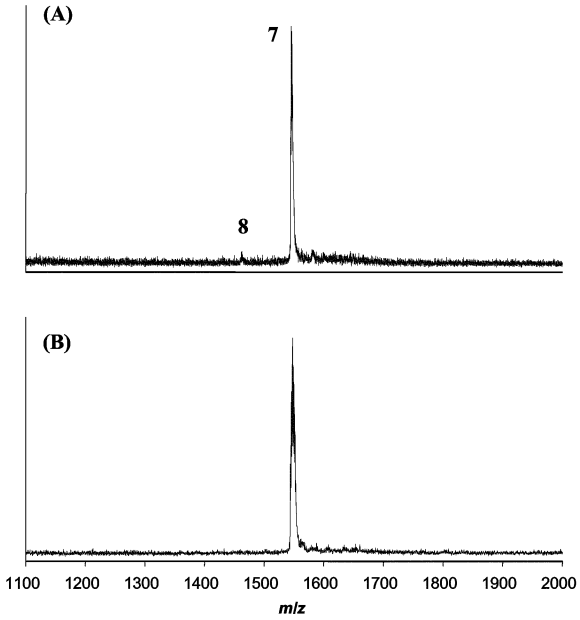

Fig. 3 (A) LD-MS spectrum of the dyad fraction from competition experiments performed at 35 °C. (B) MALDI-MS spectrum of the dyad fraction from competition experiments performed at 22 °C. Dyad **8** (undesired) is the product of bromo + ethyne coupling. Only dyad **7**, the product of iodo + ethyne coupling, is detected.

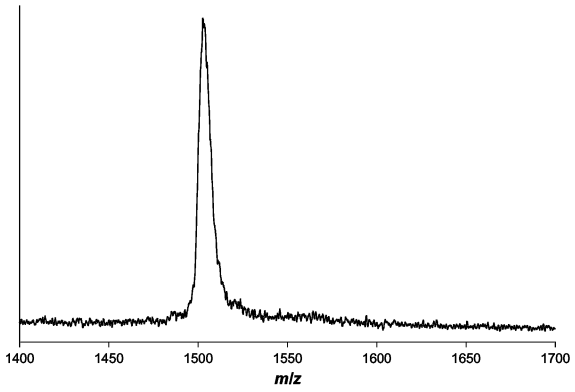

Fig. 4 LD-MS spectrum of purified dyad **9** (reaction temperature = 80 °C).

labile magnesium chelate (Scheme 6). SEC analysis showed 36% dyad formation within 1 h of reaction.[30] This value increased to only 38% after 2 h; therefore, a second batch of $Pd_2(dba)_3$ and P(*o*-tol)$_3$ was added. After 3.5 h total reaction time, the analytical SEC showed a 77% yield of dyad, a significant improvement compared to the 1 and 2 h timepoints. Importantly, the percentage of HMWM was much lower than the previous experiment, which is likely due to the reduced reaction temperature and/or higher ratio of ligand to palladium employed. Chromatographic workup afforded dyad **10** in 75% yield. The ^{1}H NMR and LD-MS spectra of dyad **10** showed no detectable impurities (see Electronic Supplementary Information†). Although additional amounts of palladium and phosphine ligand were employed to obtain the high yield, this procedure demonstrates clean Sonogashira coupling of bromo + ethynyl porphyrins under gentle reaction conditions.

Porphyrin light-harvesting rods. We have prepared three multiporphyrin arrays that are designed to meet the criteria for

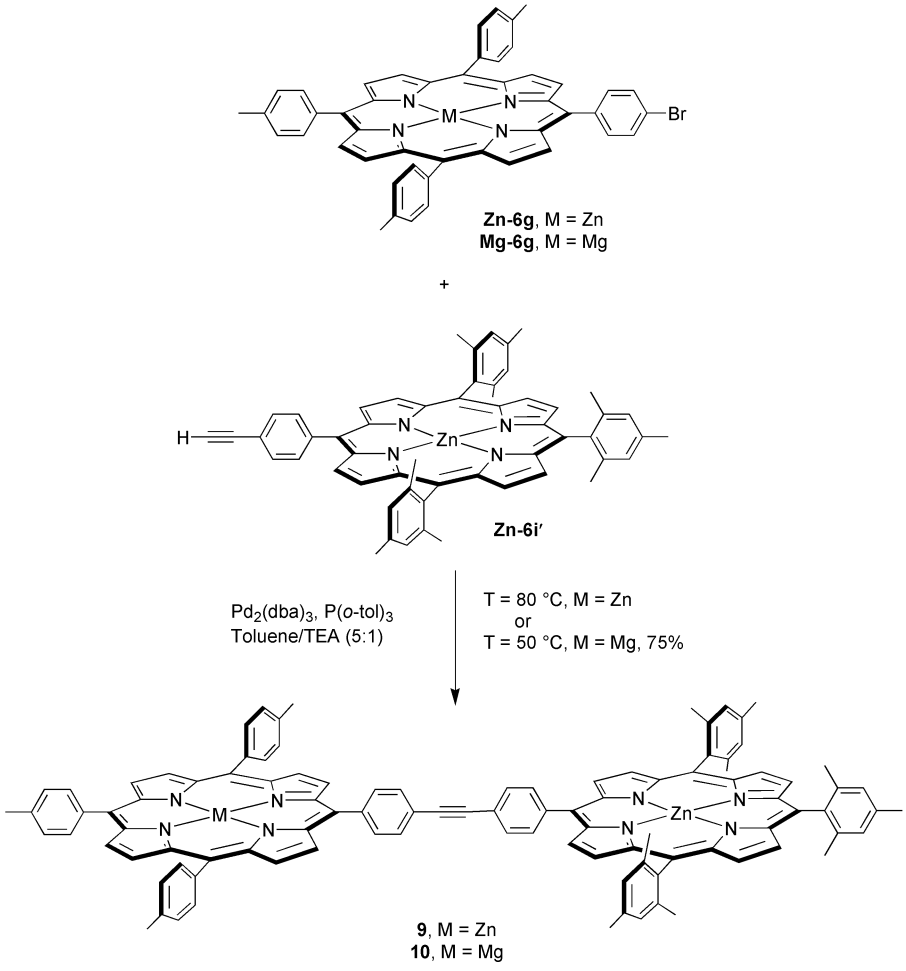

Scheme 6

intrinsic rectification of the migration of excited-state energy and ground-state holes. The terminal unit in each array is a bis(pentafluorophenyl)magnesium porphyrin bearing one carboxy group. The procedures developed for successive Sonogashira coupling of iodo- and bromo-substituted porphyrin building blocks have been employed where possible. In each case, the porphyrin array was characterized by absorption spectroscopy, fluorescence spectroscopy, mass spectrometry, TLC, analytical SEC, and where solubility permitted, by ^{1}H NMR spectroscopy.

Triad 12. The synthesis of triad **12** is shown in Scheme 7. The synthesis of a triad does not offer the possibility for convergence; therefore, we utilized stepwise Sonogashira coupling of iodo-porphyrin and ethynyl-porphyrin building blocks. Although the synthesis could be initiated from either terminus, we introduced porphyrin **Mg-6e** in the last coupling step to minimize the handling of magnesium porphyrins. Monoporphyrin building blocks **Zn-6a′** and **Zn-6b** were reacted under standard Pd-coupling conditions developed in our lab.[25] Under these conditions, the trimethylsilylethynyl-functionalized dyad was isolated in 57% yield. Removal of the trimethylsilyl protecting group using TBAF in THF furnished porphyrin dyad **11′** in 91% yield. Dyad **11′** was then allowed to react with porphyrin **Mg-6e** to produce the desired porphyrin triad **12** in 75% yield. Triad **12** was purified according to a three-column procedure: (1) one alumina column [$CHCl_3$–hexanes (4 : 1)] to remove palladium and most of the ligand, (2) one SEC column (THF) to recover the almost pure porphyrin triad, and (3) one alumina column [$CHCl_3$–hexanes (4 : 1) with slow enrichment with THF] for final purification. Triad **12** was found to be poorly soluble in $CHCl_3$ and CH_2Cl_2, but moderately soluble in THF and toluene.

Deprotection of **12** was achieved using TBAF in DMF–THF (1 : 1). After 24 h, LD-MS showed no starting material. Isolation of the product was achieved by filtration followed by washing the solid with copious amounts of water, then methanol to yield **12′** in 72% yield. The carboxy-terminated array has the ability to bind to semiconductor substrates, allowing for evaluation of solar cell performance.

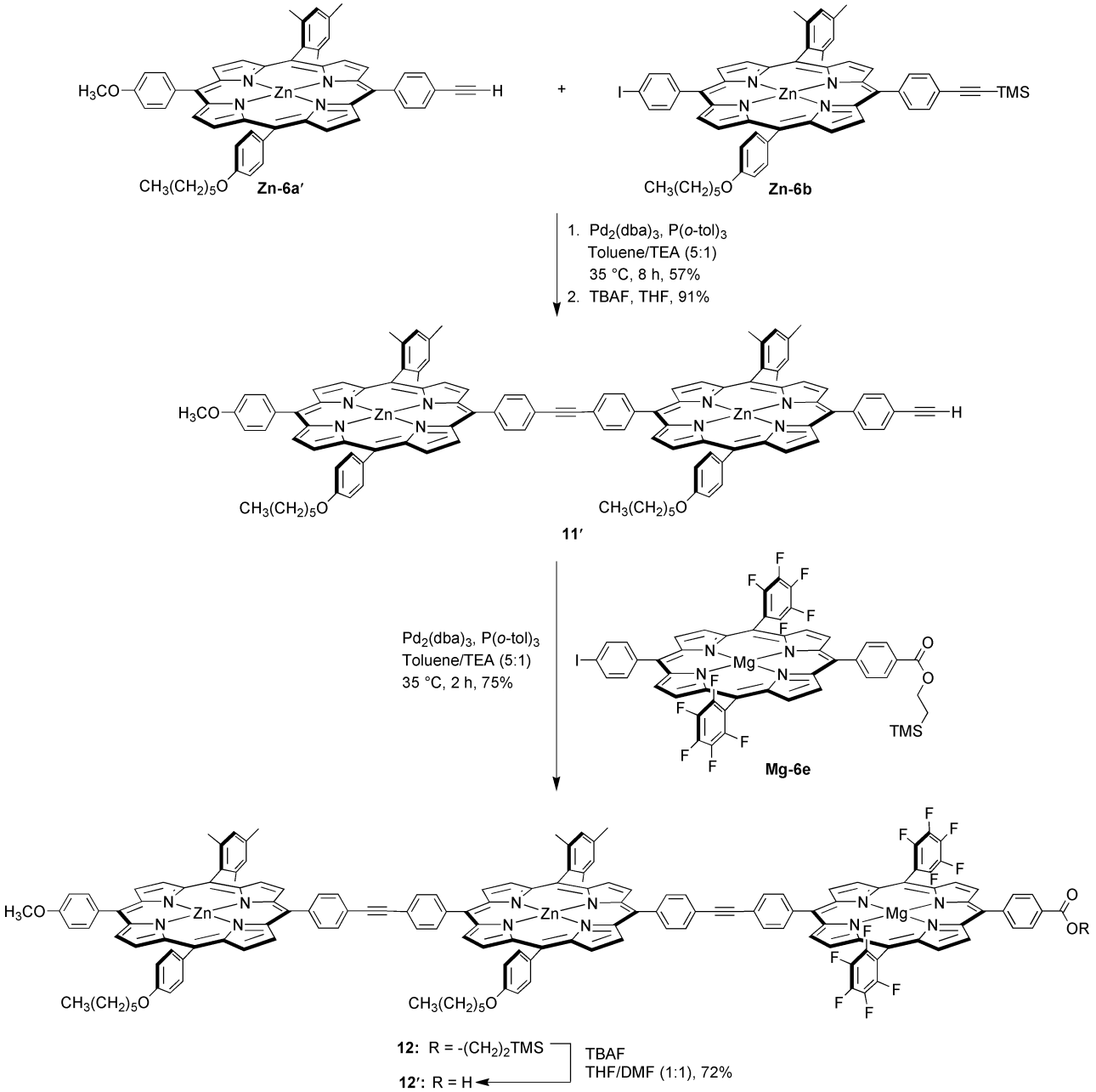

Scheme 7

*Tetrad **14***. The convergent synthesis of tetrad **14** *via* successive iodo + ethyne and bromo + ethyne coupling reactions is shown in Scheme 8. Selective Sonogashira coupling of bromo/ethynyl-porphyrin **Zn-6c′** and iodo-porphyrin **Mg-6e** at room temperature afforded bromo-porphyrin dyad **13** in 60% yield. Convergent coupling of dyad **13** and ethynyl-porphyrin dyad **11′** at 50 °C for 5 h yielded tetrad **14** in 43% yield. The solubility of **14** was poor in chlorinated solvents; the best solubility was observed with mixtures of toluene and THF. Tetrad **14′** was prepared in 50% yield by deprotection of **14** using TBAF in THF–DMF (10 : 1) at 60 °C for 17 h.

*Pentad **18***. Two routes to pentad **18** were investigated. In the first route, the successive coupling procedures were employed in a convergent route (Scheme 9). Dyad **15** was prepared by chemoselective Sonogashira coupling of bromo/ethynyl **Zn-6c′** and iodo/trimethylsilylethynyl **Zn-6d** in 60% yield. Bromo/trimethylsilylethynyl dyad **15** and ethynyl dyad **11′** were then reacted at 50 °C for 5 h to furnish tetrad **16** in 31% yield. Tetrad **16** proved to have poor solubility.[31] In a mixture of toluene and THF, one preparative SEC column afforded good separation of HMWM, product and dyadic starting materials. Characterization by ^{1}H NMR spectroscopy proved difficult, but TLC analysis showed only one spot under a variety of solvent systems, analytical SEC showed a single sharp peak, and LD-MS analysis showed a strong molecule ion peak (m/z = 3356). Because of the limited solubility, deprotection of **16** and subsequent coupling with **Mg-6e** was not attempted and a second route to prepare pentad **18** was undertaken.

The synthesis of pentad **18** *via* a convergent 3 + 2 route is shown in Scheme 10. Bromo/ethynyl-porphyrin dyad **15′** was prepared in 84% yield by treatment of **15** with TBAF in THF at room temperature for 1 h. Dyad **15′** was then reacted with **Mg-6e** at room temperature for 4.5 h to achieve selective iodo + ethyne coupling, yielding triad **17** in 51% yield. Triad **17** and dyad **11′** were then reacted in the presence of $Pd_2(dba)_3$ and P(*o*-tol)$_3$ at 55 °C. SEC analysis of an aliquot removed from the crude reaction mixture after 70 min showed 25% conversion to pentad. After another addition of catalyst and reaction for an additional 1.5 h (3 h total reaction time), analytical SEC revealed 38% conversion to pentad.[30] The reaction mixture was no longer homogeneous at this point and the reaction was stopped after 5 h. The SEC trace showed a large number of closely eluting peaks (see Experimental Section). The mixture exhibited poor solubility. Large material losses occurred upon workup and only a small amount of material (pure by SEC) was obtained. The small amount of material obtained was sufficient for initial spectroscopic characterization.

Benchmark compounds. The assessment of the electrochemical and photodynamic properties of the triad and tetrad requires suitable benchmark compounds for comparison purposes. A dyad that represents the carboxy-containing end of the triad and tetrad was prepared as shown in Scheme 11. The Pd-mediated coupling of ethynyl porphyrin **Zn-6i′** and iodo/ester porphyrin **Mg-6f** afforded the requisite ZnMg dyad **19**. Several porphyrin monomers employed in the synthesis of the arrays proved to be suitable models for analogous components of the arrays. A *trans*-diethynyl Zn porphyrin (**Zn-6j**) was used as a model for the analogous Zn porphyrin in the tetrad. These porphyrins are displayed in Chart 1. Other porphyrin monomers such as **ZnU** and **MgU** were prepared previously, as was the dyad **ZnMgU** which bears mesityl groups at all non-linking meso positions (Chart 2).

3 Physical properties of porphyrin light-harvesting rods

Electrochemistry. The $E_{1/2}$ values for the first oxidation of the series of benchmark Zn and Mg porphyrins are included in Table 1. As was noted above, the redox characteristics of these porphyrins provide a guide to the choice of building blocks for the light-harvesting rods. The trends observed for redox characteristics of these benchmark porphyrins are consistent with those of previous studies of metalloporphyrins.[16,18] These trends are as follows: (1) For a particular porphyrin, the Zn complexes are more difficult to oxidize than the Mg analogs. (2) The introduction of electron withdrawing/donating substituents raises/lowers the $E_{1/2}$ values. Thus, through a judicious choice of metal and substitution pattern essentially any potential between 0.25 and 1.0 V can be achieved.

The $E_{1/2}$ values for the first oxidation of the synthetic building blocks of the light-harvesting rods (see Chart 2) are included in Table 2. These values, beginning with the anode-terminal, electron-injecting unit (**Mg-6f**), proceeding through the transmission elements (**Zn-6j** and **Zn-6b**), and ending with the cathode-terminal, hole-injecting unit (**Zn-6a′**), are as follows: **Mg-6f**, $E_{1/2}$ = 0.60 V; **Zn-6j**, $E_{1/2}$ = 0.68 V; **Zn-6b**, $E_{1/2}$ = 0.57 V; **Zn-6a′**, $E_{1/2}$ = 0.54 V. These $E_{1/2}$ values monotonically decrease down the series **Mg-6f** > **Zn-6b** > **Zn-6a′**, as is required for migration of the hole from the anode-terminal (electron-injecting) unit to the cathode-terminal (hole-injecting) unit in a short light-harvesting rod, such as the triad **12**.

The fact that the $E_{1/2}$ value for the transmission element **Zn-6j** is larger by ~80 mV than that for the anode-terminal unit **Mg-6f** might at first glance appear to restrict hole migration in tetrameric and longer light-harvesting rods, **14** and **18**, respectively. However, this is not the case for the following reasons: (1) The $E_{1/2}$ value for the transmission element in the actual rod is lower than that for the building block **Zn-6j**. In the rod, each of the two ethyne hydrogens of **Zn-6j** is replaced by the phenyl ring of an adjacent porphyrin. Previous studies of multiporphyrin arrays have shown that the substitution of a phenyl ring for hydrogen lowers the $E_{1/2}$ value by ~30 mV per phenyl ring.[7] Thus, the $E_{1/2}$ value of the transmission element that is adjacent to the anode-terminal unit in an actual rod is within 20 mV of the $E_{1/2}$ value of this latter unit. This value is less than thermal energy at ambient temperature; thus, facile hole migration should occur in this last segment as in the entire rod. (2) Previous studies of hole hopping in multiporphyrin arrays wherein two Zn porphyrins are separated by a Fb porphyrin have shown that the hole rapidly hops between the Zn porphyrins (at a rate $>10^7$ s^{-1})[7,8] despite the fact the redox potential of the intervening Fb porphyrin is much higher (>200 mV) than that of the Zn porphyrin.[16] The rapid hopping occurs because the Fb porphyrin serves as superexchange mediator (rather than acting as a cationic intermediate).[7,8,19] Accordingly, the presence of a small uphill redox gradient in a segment of a light-harvesting rod wherein the overall end-to-end gradient is downhill should not impede hole migration.

Finally, we note that the $E_{1/2}$ value of the cathode-terminal building block **Zn-6a′** is also skewed more positive than that for the analogous unit of an actual rod, again by the presence of an ethynyl hydrogen in the building block (Chart 1). On the other hand, the presence of iodo (*vs.* ethynylphenyl) and trimethylsilyl (*vs.* phenyl) groups in the building block **Zn-6b** makes the potential slightly less positive than the $E_{1/2}$ value of the transmission element.[32] Thus, the overall end-to-end electrochemical gradient in the light-harvesting rod is actually more favorable for hole migration than would be suggested by the $E_{1/2}$ values of the building blocks.

Static absorption spectra. The electronic ground-state absorption spectrum of the ZnMg dyad **19** is shown in Fig. 5A (solid spectrum). This figure also shows spectra of monomeric Mg and Zn reference porphyrins (**Mg-6f** and **ZnU**), which contain the same substituents at the non-linking positions as in the dyad (panels B and C). The spectra of the monomers contain the typical metalloporphyrin features, namely the intense near-UV Soret (B) band, corresponding

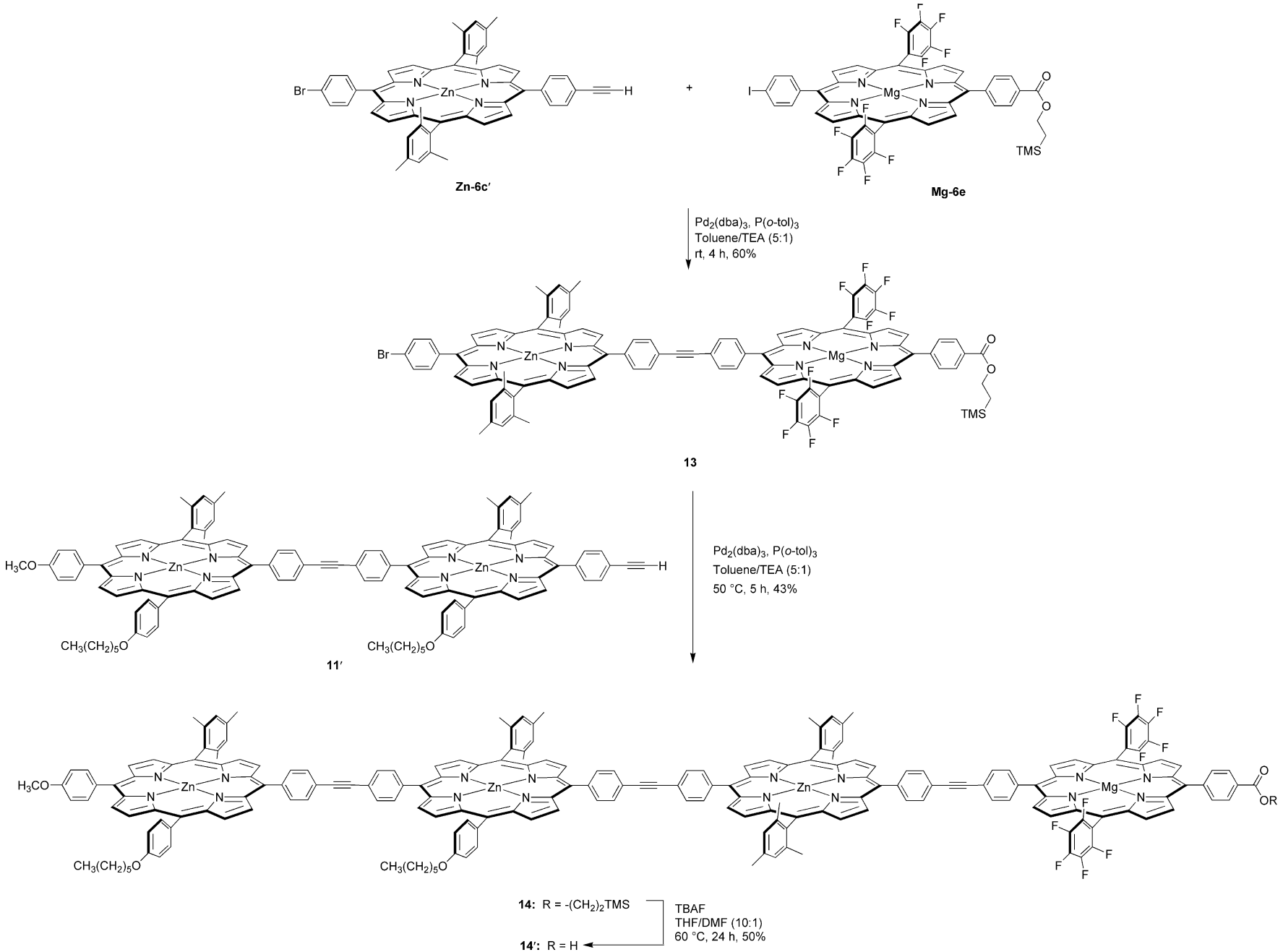
Zn-6c′
Mg-6e
Pd2(dba)3, P(o-tol)3
Toluene/TEA (5:1)
rt, 4 h, 60%
13
11′
Pd2(dba)3, P(o-tol)3
Toluene/TEA (5:1)
50 °C, 5 h, 43%
14: R = -(CH2)2TMS
14′: R = H
TBAF
THF/DMF (10:1)
60 °C, 24 h, 50%

Scheme 8

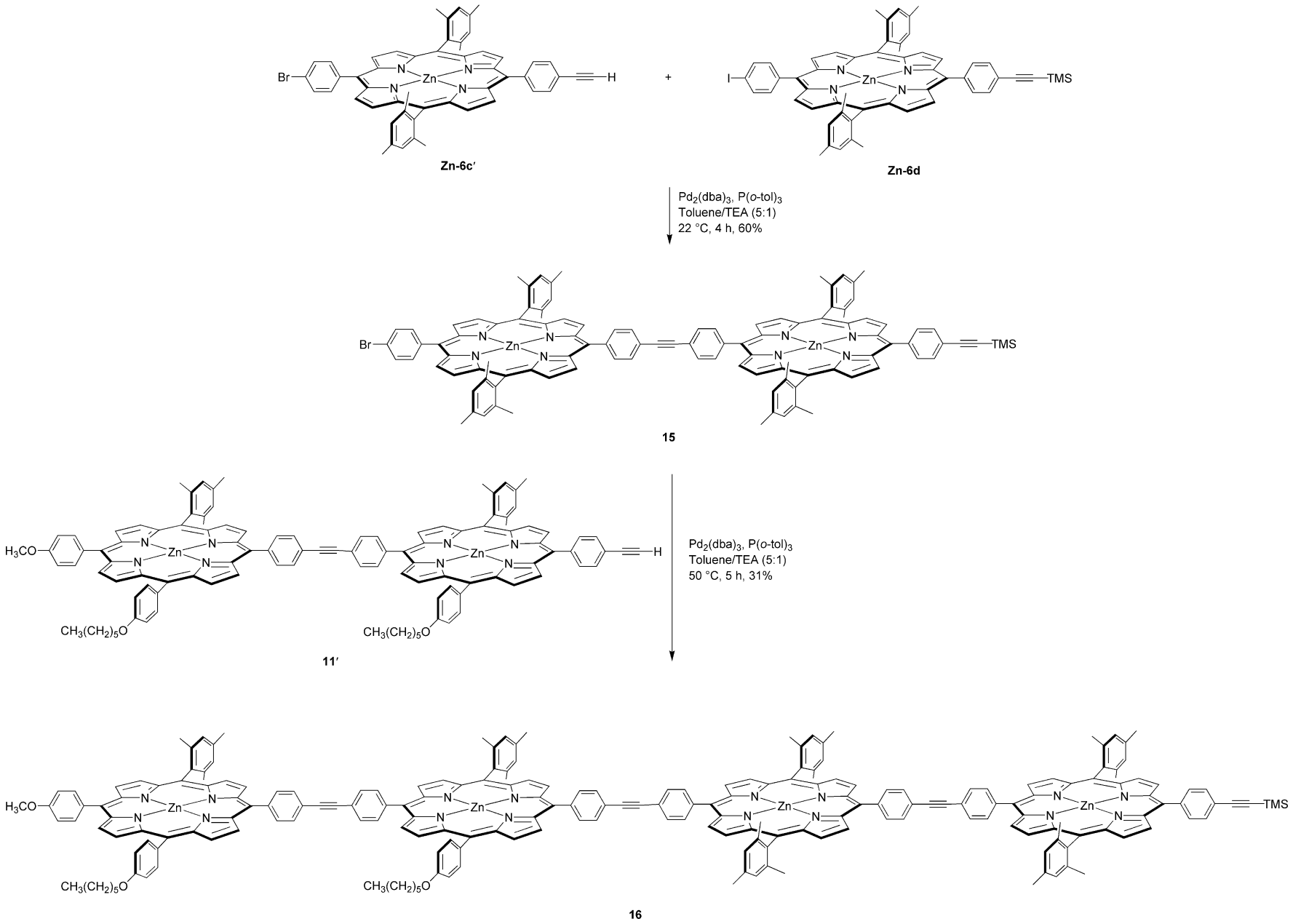
Br
H
Zn-6c′
I
TMS
Zn-6d
Pd2(dba)3, P(o-tol)3
Toluene/TEA (5:1)
22 °C, 4 h, 60%
15
H3CO
CH3(CH2)5O
11′
Pd2(dba)3, P(o-tol)3
Toluene/TEA (5:1)
50 °C, 5 h, 31%
16

Scheme 9

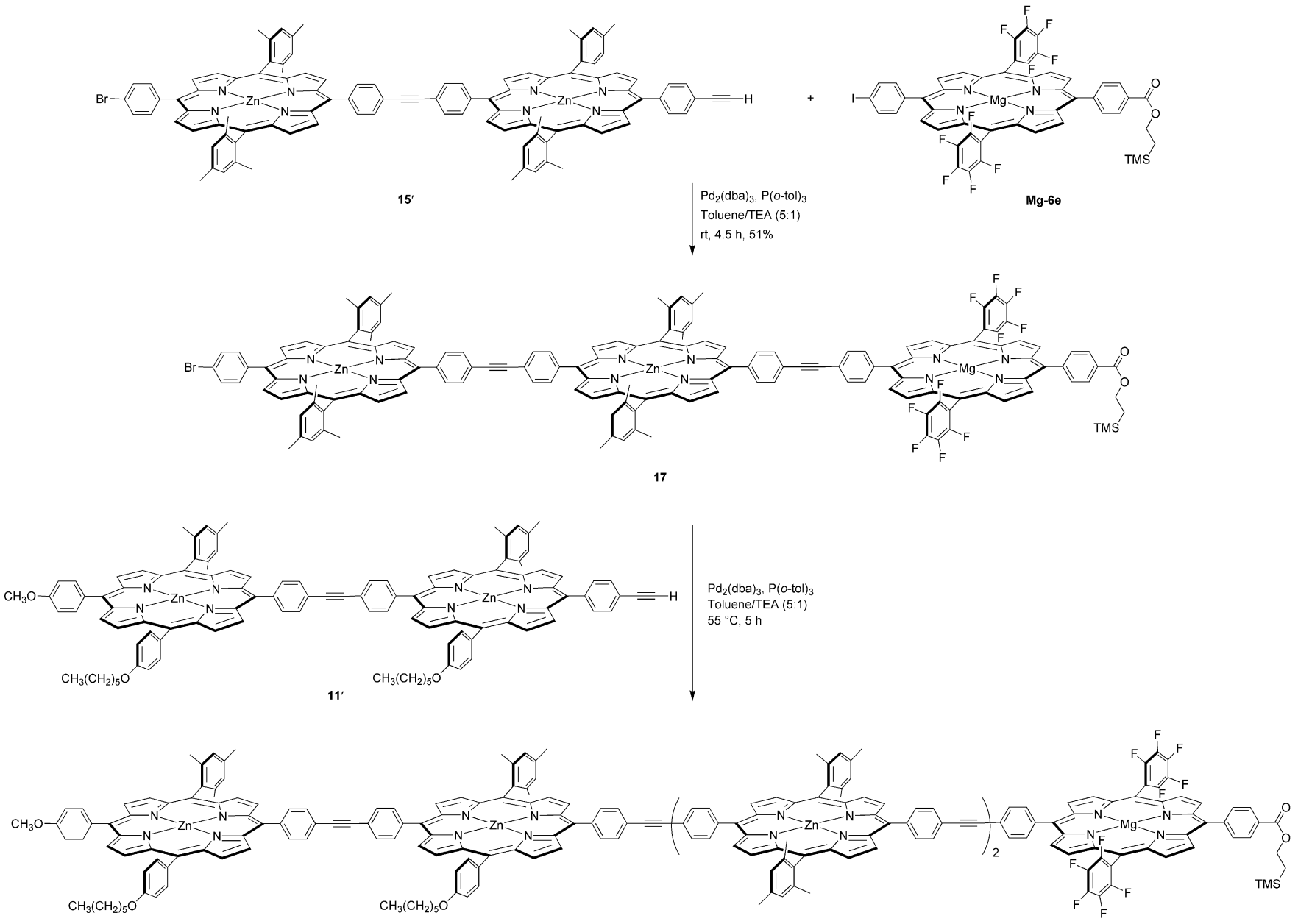
15′
Mg-6e
Pd2(dba)3, P(o-tol)3
Toluene/TEA (5:1)
rt, 4.5 h, 51%
17
11′
Pd2(dba)3, P(o-tol)3
Toluene/TEA (5:1)
55 °C, 5 h
18

Scheme 10

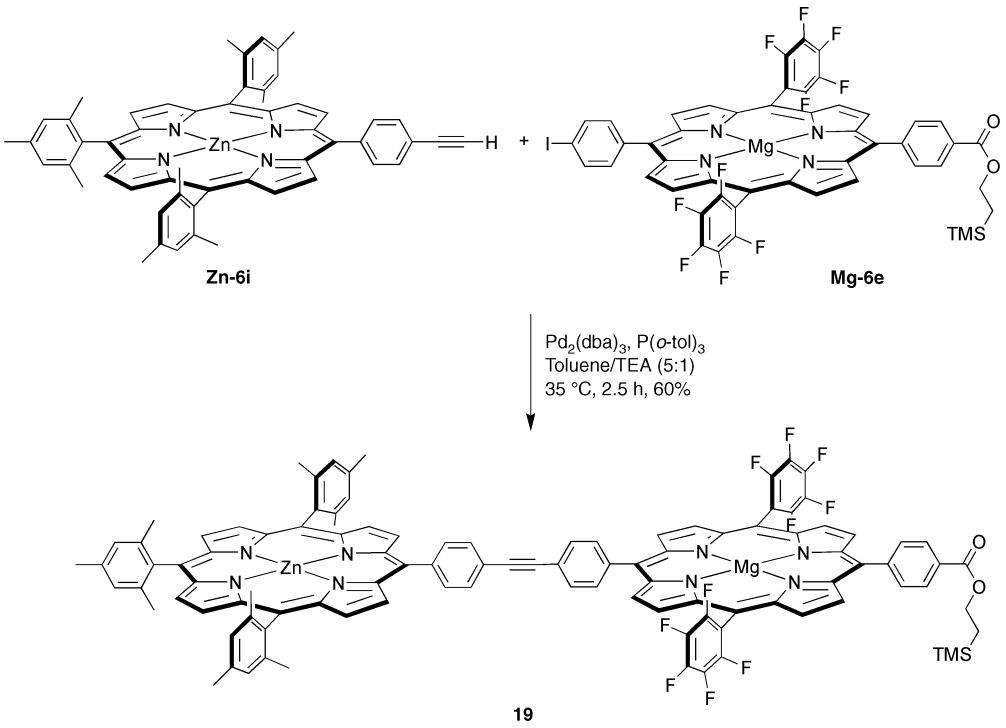

Scheme 11

to the $S_0 \rightarrow S_2$ transition, and a series of weaker visible bands — Q(2,0), Q(1,0), and Q(0,0) — corresponding to the $S_0 \rightarrow S_1$ transition. These four features are at approximately 423, 510, 550 and 590 nm for the Zn porphyrin and 426, 520, 560, and 605 nm for the Mg porphyrin in toluene. The positions of the Q(0,0) absorption bands, like the Q(0,0) fluorescence features described below, indicate that the lowest excited singlet state of the Mg porphyrin lies $\sim$0.05 eV lower in energy than that of the Zn porphyrin. This energy difference is an essential design criterion to ensure the flow of excited-state energy from the Zn porphyrin(s) to the terminal Mg porphyrin when the units are joined in the light-harvesting rods (Fig. 1).

This energy gradient is retained in the dyad **19**, as is seen from the presence of the Q(0,0) bands of the Mg and Zn porphyrins at the positions found in the reference monomers (Fig. 5). In fact, the entire Q-band manifold of the dyad is essentially the sum of the spectra of the component parts. We have extensively documented this important characteristic of diarylethyne-linked porphyrins, which is retained even in branched arrays containing 21 porphyrins.[33] The unchanged position of each of the Q bands in the dyad reflects the relatively weak (though significant) electronic coupling between the lowest excited singlet states of the porphyrin components. On the other hand, exciton coupling between the strong B-transition dipoles of the component porphyrins causes the near-UV region of the dyad spectrum to deviate from the sum of the monomer bands. This coupling results in a splitting and shift in the center of gravity of the composite Soret band from the monomer-band average; these properties are seen in the spectrum of the ZnMg dyad **19** in Fig. 5 and are even more evident in dyads containing identical subunits studied here and previously.[9]

These results demonstrate that although the $S_0 \rightarrow S_2$ transitions of the component diarylethyne-linked porphyrins are strongly coupled, the electronic characteristics designed into the photophysically relevant lowest excited singlet states of the monomeric building blocks are retained in the ZnMg dyad. The same is found to be true for Zn_2Mg triad **12** and Zn_3Mg tetrad **14**, and can be extrapolated with confidence to progressively longer light-harvesting rods. The same properties are retained when the arrays are placed in solvents of increasing polarity and increasing ability to coordinate to the central metals of the metalloporphyrins, such as tetrahydrofuran (THF) and acetonitrile (MeCN). In these polar solvents, mainly due to metal-coordination effects, the energy gradient from Zn to Mg porphyrin units is reduced compared to nonpolar, non-ligating solvents such as toluene (more so in MeCN than THF), but is still present. The latter fact, in addition to other standard metal-coordination effects, is seen from the absorption spectra, as well as the static emission and time-resolved absorption data described below. These issues were examined because polar (and metal-coordinating) media may be used for some applications of the light-harvesting rods.

Emission spectra, quantum yields, and lifetimes. The emission spectra of ZnMg dyad **19** and its component reference monomers, **Mg-6f** and **ZnU**, in toluene are shown in Fig. 5 (dashed spectra). In analogy with the absorption spectra, the Q(0,0) and Q(0,1) emission bands of the monomeric Mg porphyrin (609 and 662 nm) are $\sim$15 nm to longer wavelengths than those of the reference Zn porphyrin (594 and 645 nm). Thus, the relative Q(0,0) emission positions again reflect the $\sim$0.05 eV lower energy of the lowest excited singlet state of the Mg *versus* Zn porphyrin.

One of the most noteworthy findings is that emission from ZnMg dyad **19** occurs predominantly from the Mg porphyrin component, regardless of excitation wavelength (Fig. 5A). Although fully selective optical pumping of either component is not possible due to spectral overlap, absorption at 549 nm on the blue side of the dyad's Q(1,0) feature should favor excitation of the Zn porphyrin while 562 nm photons on the red side of the band should favor excitation of the Mg porphyrin. Regardless, there is no evidence for Zn-porphyrin emission from the dyad even when using 549 nm excitation. This can be seen by comparison of the spectra in Fig. 5, and the finding that the spectra using 549 and 562 nm excitation are superimposable (not shown). Furthermore, the emission intensity (from the Mg porphyrin) is comparable when the excitation favors either the Zn porphyrin or Mg porphyrin (when corrected for different absorbances at the excitation wavelengths). Similar results for dyad **19** are found in THF and MeCN. Similar results also were obtained for Zn_2Mg triad **12**

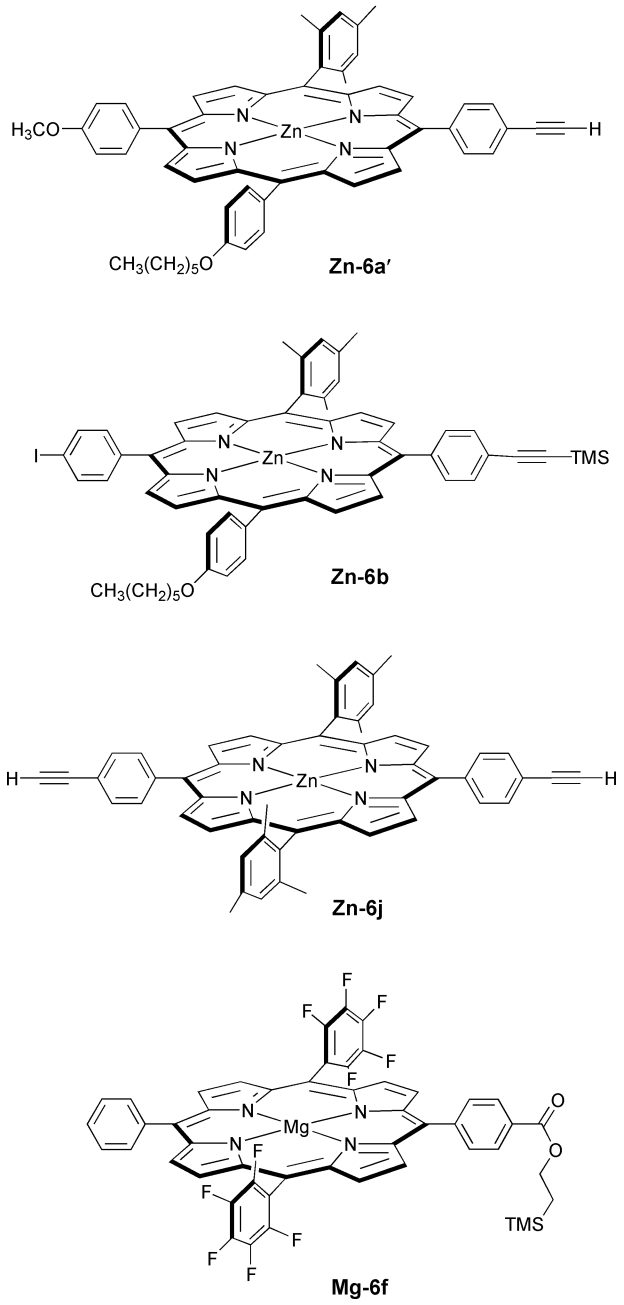

Chart 1

and Zn_3Mg tetrad **14** in THF, a solvent in which these arrays are more soluble than in toluene. These results are all indicative of efficient energy transfer from the excited singlet state of the Zn porphyrin (Zn*) to the ground-state Mg porphyrin to form Mg*.[34] Facile Zn*Mg → ZnMg* energy transfer is further demonstrated by the transient absorption data described below. For the triad and tetrad, the results also show that energy input at the distant Zn porphyrin(s) migrates efficiently to the terminal Mg porphyrin.

The fluorescence quantum yields and lifetimes of dyad **19**, triad **12** and tetrad **14** and monomeric reference compounds are summarized in Table 3. The emission yields and lifetimes for monomers **Mg-6f** ($\Phi_f = 0.14$, $\tau = 8.3$ ns) and **MgU** ($\Phi_f = 0.16$, $\tau = 9.7$ ns)[35] in toluene show that the addition of two pentafluorophenyl rings (to properly poise the porphyrin redox potential for use in the light-harvesting rods) does not significantly affect the intrinsic excited-state properties of the Mg porphyrin.[36] For dyad **19** in toluene, the emission yield and excited-state lifetime of the Mg porphyrin are reduced by 30–40% relative to that of the reference compound **Mg-6f** ($\Phi_f = 0.087$ *versus* 0.14; $\tau = 6.0$ ns *versus* 8.3 ns). The values are more substantially reduced in the dyad *versus* monomer in MeCN ($\Phi_f = 0.061$ *versus* 0.13; $\tau = 2.6$ *versus* 7.6 ns).[37] The reduced emission and lifetime in **19** and the dependence on solvent polarity indicate that Mg* in this dyad decays in part *via* a channel not present in the Mg porphyrin monomer, namely charge transfer involving the Zn porphyrin component. The electrochemical data described above indicate that the most viable charge-transfer process is $ZnMg^* \rightarrow Zn^+Mg^-$ hole transfer. Using the standard analysis of the emission yield and lifetime data,[38,39] the hole-transfer efficiencies and rate constants for dyad **19** are found to be ~35% and $(24\ ns)^{-1}$ in toluene and ~60% and $(13\ ns)^{-1}$ in MeCN. This process of hole transfer from the excited state of the Mg porphyrin is analogous but not identical to the ground-state hole-transfer process that is expected to occur following electron-injection by Mg* into a semiconductor.

The decay of Mg* in dyad **19** due to hole transfer to the Zn porphyrin (rather than electron transfer or no charge transfer at all) is a consequence of the redox-potential tuning caused by the inductive effect of the two pentafluorophenyl rings on the Mg porphyrin (Tables 1 and 2). The combined effects of the porphyrin substituents clearly have moved the Zn^+Mg^- charge-separated state somewhat below the energy level of Mg* in dyad **19** even in nonpolar media such as toluene, and no doubt farther below in polar media such as MeCN.[40,41] As noted above, the movement of holes from the Mg to Zn porphyrin(s) is a key characteristic for the rectification effect in the light-harvesting rods (Fig. 1). A limited extent of charge transfer in the excited state of the Mg porphyrin may facilitate electron injection into a semiconductor (by Mg^- rather than Mg*) and ensuing hole transfer down the Zn-porphyrin chain. The fact that Mg* remains very long lived (6 ns in nonpolar toluene and 2.6 ns in highly polar MeCN) ensures ample time for efficient excited-state electron injection in the solar cells in a range of media.

Time-resolved absorption spectroscopy. The rate of energy flow from the Zn porphyrin(s) to the Mg porphyrin was examined for dyad **19**, triad **12**, and tetrad **14**. Fig. 6 shows representative data for dyad **19** in THF, obtained using 130 fs excitation flashes at 595 nm. The absorption difference spectrum shown at 2 ps after excitation contains the typical characteristics of metalloporphyrin excited states.[42] These features include strong excited-state absorption immediately to the red of the Soret-band bleaching that tails to longer wavelengths and is broken by the bleaching of the ground-state Q bands. The Q(1,0) bleaching at 2 ps is centered at ~560 nm but shows a distinct shoulder at ~570 nm. Based on the static optical properties described above, the former can be assigned mainly to Zn* and the latter to Mg*, with each state formed by direct excitation in independent fractions of the arrays due to spectral overlap with the 595 nm excitation flash. At 250 ps, the bleaching on the shorter wavelength side of the feature has decayed and that at longer wavelengths has grown. These spectral changes are indicative of Zn*Mg → ZnMg* energy transfer. The excited Mg porphyrins thus formed (and those produced by direct excitation) do not decay appreciably over the 500 ps time course of these experiments, consistent with the multi-nanosecond Mg* lifetimes found above from the fluorescence measurements. The inset to Fig. 6 shows a typical kinetic trace and a fit to a single exponential function with a time constant of 9 ± 2 ps. This value can be assigned to the Zn* lifetime for dyad **19** in THF.

Similar results are found for triad **12** and tetrad **14** in THF, except that the Zn* lifetime lengthens to 15 ± 3 ps and 30 ± 8 ps, respectively. The progressively longer excited-state lifetime with increasing number of Zn porphyrins in the rod reflects the fact that excitation will produce a Zn* increasingly farther from the Mg porphyrin, thereby requiring more

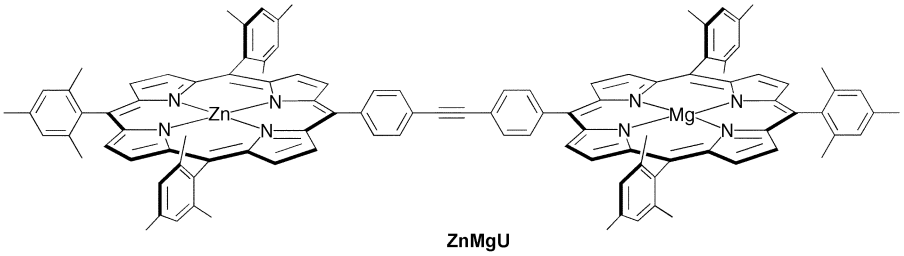

ZnMgU

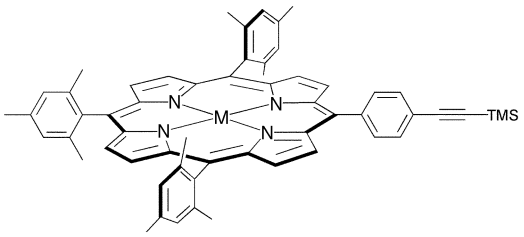

ZnU, M = Zn

MgU, M = Mg

Chart 2

Table 2 Q(0,0) Absorption maxima and electrochemical data for Zn and Mg porphyrins

Porphyrin	λ_{abs} Q(0,0)[a]	$E_{1/2}$/mV[b]
Zn-6a′	593	0.54
Zn-6b	593	0.57
Zn-6j	590	0.68
Mg-6f	604	0.60

[a]In toluene. [b]$E_{1/2}$ *vs.* Ag/Ag^+ in CH_2Cl_2 containing 0.1 M Bu_4NPF_6; $E_{1/2}$ of $FeCp_2/FeCp_2^+$ is 0.19 V.

intervening energy-transfer steps between Zn porphyrins.[43] Nonetheless, these Zn* lifetimes are all considerably shorter than the value of 2.4 ns for monomeric Zn porphyrins

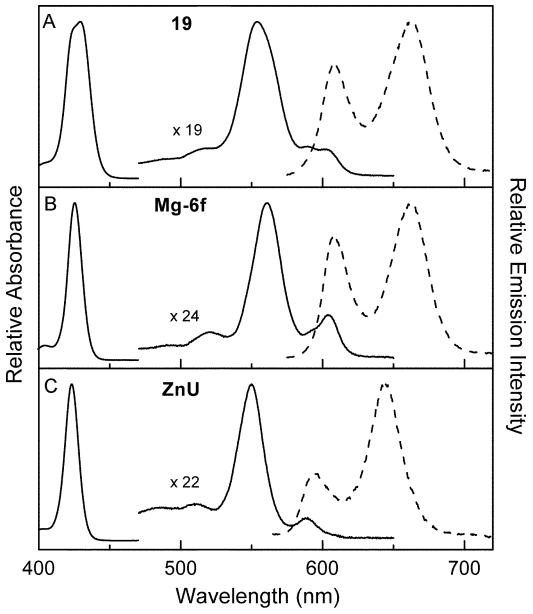

Fig. 5 Absorption (solid) and fluorescence (dashed) spectra for dyad **19**, Mg porphyrin monomer **Mg-6f**, and Zn porphyrin monomer **ZnU** in toluene at room temperature. The near-UV Soret absorption bands, the visible Q(1,0) absorption band, and the Q(0,1) fluorescence bands have been normalized to 1. For each compound, the Q-band region has been multiplied relative to the Soret band by the factor indicated.

Table 3 Photophysical data for arrays and reference compounds[a]

Compound	Solvent	Φ_F[b]	τ_{Zn*}/ps[c]	τ_{Mg*}/ns[c]
19 (**ZnMg** dyad)	Toluene	0.087	—	6.0 ± 0.6
	THF	—	9 ± 2[d]	—
	MeCN	0.061	60 ± 10[e]	2.6 ± 0.2
12 (**Zn_2Mg** triad)	THF	0.047	15 ± 3[d]	—
14 (**Zn_3Mg** tetrad)	THF	0.055	30 ± 8[d]	—
ZnMgU	Toluene	0.17[f]	9 ± 2[f]	5.8 ± 0.3[f]
	MeCN	—	55 ± 10[g]	—
Mg-6f	Toluene	0.14		8.3 ± 0.5
	MeCN	0.13		7.6 ± 0.5
Mg-6e	Toluene	0.012		—
ZnU	Toluene	0.034[h]	2400 ± 200[hi]	
	THF	—	2600 ± 200[h]	
	MeCN	0.063[h]	2400 ± 200[h]	
MgU	Toluene	0.16[h]		9.7 ± 0.4[fh]
	THF	0.18		9.7 ± 0.5[h]
	MeCN	0.19[h]		9.6 ± 0.5[h]

[a]All data were acquired at room temperature (THF = tetrahydrofuran; MeCN = acetonitrile). [b]Fluorescence quantum yields (10% error) are referenced to 0.033 for ZnTPP and 0.16 for MgTPP.[35,45] Yields for Zn monomers were determined using 549 nm excitation and those for Mg porphyrin monomers and the Mg porphyrin in each dyad using 563 nm excitation. [c]Lifetimes > 1 ns were determined by fluorescence measurements and lifetimes < 1 ns by transient absorption spectroscopy. [d]λ_{exc} = 595 nm. [e]λ_{exc} = 413 nm. There is a second component with τ = 1–4 ns that likely represents decay of Mg*, which has τ = 2.6 ns as determined by fluorescence lifetime measurements. [f]From ref 41. [g]λ_{exc} = 413 nm. [h]From ref. 35. [i]From ref. 4.

(Table 3). This finding, like the static emission data described above, indicates that energy transfer leading to the formation of Mg* dominates the decay of Zn* in these linear arrays. Using the standard analysis, these lifetimes give energy-transfer rate constants in THF of $(9\ ps)^{-1}$, $(15\ ps)^{-1}$, and $(30\ ps)^{-1}$ for ZnMg dyad **19**, Zn_2Mg triad **12**, and Zn_3Mg tetrad **14**, respectively, and a quantum efficiency $\geqslant$99% in each case.

The energy-transfer dynamics of dyad **19** were also studied in MeCN because the light-harvesting rods may be used in highly polar (and metal-ligating) media for certain applications. Transient absorption spectra similar to those obtained in THF (Fig. 6) were obtained, with the Zn* lifetime increasing to ~60 ps. Similar results were obtained for **ZnMgU**, which contains only mesityl groups at the non-linking meso positions

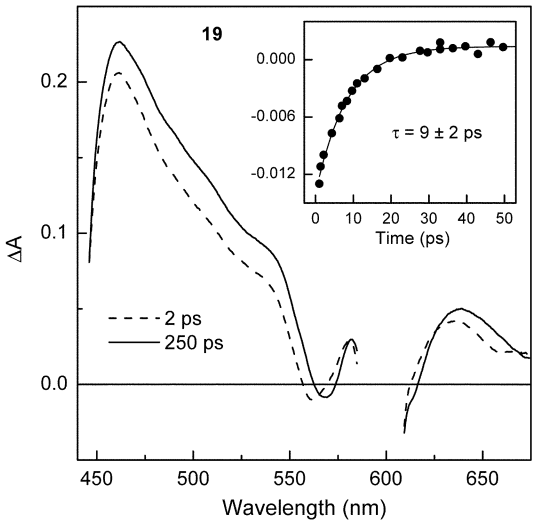

Fig. 6 Time-resolved absorption data for dyad **19** in THF at room temperature. Samples were excited with a 130 fs excitation flash at 595 nm. The line through the data in the inset is a single exponential fit with a time constant indicated; kinetic data before and during the flash and from 50 ps to 500 ps are not shown for clarity.

(rather than the other substituents including two pentafluorophenyl substituents on the Mg porphyrin in **19**). These findings indicate that the modest lengthening of the Zn* lifetime derives primarily from solvent interactions (including metal ligation effects), and that these effects are not a consequence of the peripheral groups used to tune the redox properties of the components in the light-harvesting rods. A Zn* lifetime of 60 ps compared to the 2.4 ns value in reference monomers corresponds to a rate constant of $(62\ \text{ps})^{-1}$ and a quantum efficiency of 98% for the Zn*Mg → ZnMg* energy-transfer process. These results indicate that the light-harvesting rods have robust energy-transfer characteristics that are maintained under a variety of conditions for use in solar-energy applications.

Conclusions

A new design has been developed for components of a molecular solar cell. The design specifies a molecular rod comprised of pigments chosen for light absorption and the support of the migration of excited-state energy and ground-state holes in opposite directions. The challenge of constructing such components motivated the development of new synthetic methodologies based on successive iodo + ethyne and bromo + ethyne coupling reactions, which enabled a degree of convergence to be employed in the synthesis of multiporphyrin arrays. Porphyrin building blocks with the desired spectral, electrochemical, and attachment groups were identified and synthesized. The building blocks were employed in a stepwise, rational synthesis of linear arrays comprised of 3-5 porphyrins in the backbone of the array. The porphyrin oligomers exhibit all the key features necessary for construction of a viable molecular solar cell: absorption of visible light, efficient excited-state energy migration in one direction along the rod, an electrochemical gradient for reverse migration of ground-state holes, and a linker for surface attachment.

Experimental

General

^{1}H (300 MHz) and ^{13}C (75 MHz) NMR spectra were recorded in $CDCl_3$ unless noted otherwise. Mass spectra of porphyrins were obtained by high-resolution fast atom bombardment (FAB), by laser desorption mass spectrometry (LD-MS), or by LD-MS in the presence of the matrix POPOP (MALDI-MS). Absorption spectra were collected in toluene unless noted otherwise. Elemental analyses were performed by Atlantic Microlab, Inc. Melting points are uncorrected. Silica gel (Baker 40 μm average particle size) and alumina (Fisher, 80–200 mesh) were used for column chromatography. Preparative SEC was performed using BioRad Bio-Beads SX-1 (200–400 mesh) beads. Analytical SEC was performed using an HP 1090 Liquid Chromatograph (column size = 1000 Å; flow rate = 0.800 mL min^{-1}; solvent = THF; quantitation at 420 nm; oven temperature 40 °C). Tris(dibenzylideneacetone)dipalladium(0) [$Pd_2(dba)_3$], tri-*o*-tolylphosphine [P(*o*-tol)$_3$], and all other reagents were purchased from Aldrich and used as received. Room temperature was determined to be 21–22 °C using a calibrated thermometer (Fisher).

Palladium coupling reactions

All Pd-mediated reactions were performed using a Schlenk line. Standard pump-purge methods were employed to achieve reaction under anaerobic conditions.[25] Toluene and triethylamine (TEA) were freshly distilled from CaH_2 and sparged of oxygen prior to use. The reactions were performed in dilute solution in the absence of any copper reagents.[24] Palladium insertion and transmetalation have not been observed with these conditions.

Electrochemical studies

The electrochemical studies were performed using techniques and instrumentation previously described.[7] For all the porphyrins, the solvent was CH_2Cl_2 and 0.1 M Bu_4NPF_6 (Aldrich, recrystallized three times from methanol and dried under vacuum at 110 °C) served as supporting electrolyte. The potentials were measured *vs.* Ag/Ag^+; $E_{1/2}(FeCp_2/FeCp_2^+)$ = 0.19 V. The scan rate was 0.1 V s^{-1}.

Static and time-resolved optical studies

Static absorption, static emission, fluorescence lifetime, and time-resolved absorption measurements on samples at room temperature were performed as described previously.[6,44] Fluorescence lifetime measurements utilized samples that were deoxygenated by bubbling with dry N_2. Fluorescence spectra were corrected for the instrument response. Static emission and fluorescence lifetime studies utilized 0.1–2 μM samples in 10 cm cuvettes. For time-resolved absorption studies, samples (~0.1–0.2 mM in 2 mm pathlength cuvettes) were excited at 10 Hz with 130 fs pulses (4–8 μJ, 390–450 nm; 20–30 μJ, 480-590 nm) and probed with white-light flashes of comparable duration. Fluorescence quantum yields (10% error) are referenced to 0.033 for ZnTPP and 0.16 for MgTPP.[35,45]

Non-commercial compounds

Compounds **2a,b,d,e**;[21] **2f**;[46] **3**, **5c**, and **5e**;[20] **5f**;[47] **Mg-6h**;[25] **Mg-6i′** and **MgU**;[35] **Zn-6j**;[48] **ZnU**[26] and **ZnMgU**[41] were prepared as described in the literature. Compound **2c**[49] was prepared using a refined method.[21] Compounds **Zn-1a** (ZnTPP) and **Zn-1b** (ZnTMP) are standard compounds. Porphyrins **1c**;[46] **1d** and **1e**;[20] and **1f**[50] were prepared as described in the literature and were metalated as needed.

5-[4-(Hexyloxy)phenyl]dipyrromethane (2g). Following a general procedure,[21] a mixture of pyrrole (65 mL, 1.0 mol) and 4-(hexyloxy)benzaldehyde (7.94 g, 38.5 mmol) was treated with TFA (0.296 mL, 3.84 mmol). The mixture was stirred for 5 min. Ethyl acetate (70 mL) and a solution of 0.1 M aq. NaOH (70 mL) were added. The layers were separated. The aqueous layer was washed with additional ethyl acetate (50 mL). The

organic layers were collected, dried (Na_2SO_4), and concentrated. Column chromatography (silica, CH_2Cl_2) afforded a yellow, viscous oil which was recrystallized from ethanol–H_2O (10 : 1), affording an amorphous, pale yellow solid (4.88 g, 40%): mp 58–60 °C; ^{1}H NMR δ 0.91 (t, 3H), 1.33 (m, 4H), 1.46 (m, 2H), 1.77 (m, 2H), 3.94 (t, 2H), 5.42 (s, 1H), 5.92 (m, 2H), 6.15 (m, 2H), 6.69 (m, 2H), 6.85 (d, J = 8.7 Hz, 2H), 7.11 (d, J = 8.7 Hz, 2H), 7.91 (br s, 2H); ^{13}C NMR δ 14.0, 22.6, 25.7, 29.2, 31.5, 43.0, 68.0, 107.0, 108.3, 114.5, 117.0, 129.3, 132.9, 133.9, 158.0; HRMS (FAB) obsd 322.2053, calcd 322.2045. Anal. Calcd ($C_{21}H_{26}N_2O$): C, 78.22; H, 8.13; N, 8.69. Found: C, 77.32; H, 8.08; N, 8.62.

5-Mesityl-1-(4-methoxybenzoyl)-9-{4-[2-(trimethylsilyl)ethynyl]-benzoyl}dipyrromethane (5a). Following a general procedure,[20] a solution of **4a** (2.85 g, 6.13 mmol) in dry toluene (25 mL) was treated with EtMgBr (12.2 mL, 12.2 mmol, 1 M in THF) followed by 4-anisoyl chloride (1.04 g, 6.10 mmol). Second and third additions (identical amounts; half the amount, respectively) were performed after 10 and 20 min, followed by the standard workup. Chromatography [column 1: silica, CH_2Cl_2, followed by CH_2Cl_2–ethyl acetate (9 : 1); column 2: silica, ethyl acetate] afforded a red solid (2.59 g, 71%): mp 136–138 °C; ^{1}H NMR δ 0.26 (s, 9H), 2.19 (s, 6H), 2.31 (s, 3H), 3.85 (s, 3H), 6.03 (m, 2H), 6.11 (s, 1H), 6.67 (m, 2H), 6.90 (d, J = 8.1 Hz, 2H), 6.92 (s, 2H), 7.49 (d, J = 8.7 Hz, 2H), 7.70 (d, J = 8.1 Hz, 2H), 7.78 (d, J = 8.7 Hz, 2H), 10.46 (br s, 2H); ^{13}C NMR δ −0.2, 20.9, 39.2, 55.3, 96.9, 104.3, 110.3, 110.5, 113.2, 120.2, 121.1, 126.1, 129.2, 130.1, 130.3, 130.4, 130.9, 131.4, 133.2, 136.9, 137.5, 137.9, 139.1, 140.7, 162.3, 182.6. Anal. Calcd ($C_{38}H_{38}N_2O_3Si$): C, 76.22; H, 6.40; N, 4.68. Found: C, 76.06; H, 6.53; N, 4.62.

1-(4-Bromobenzoyl)-5-mesityl-9-{4-[2-(trimethylsilyl)ethynyl]-benzoyl}dipyrromethane (5b). Following a general procedure,[20] reaction of **4a** (2.79 g, 6.00 mmol) and 4-bromobenzoyl chloride (1.32 g, 6.00 mmol) followed by column chromatography (silica, CH_2Cl_2) and recrystallization (CH_2Cl_2–methanol) afforded a yellow solid (2.66 g, 68%): mp 144–146 °C; ^{1}H NMR δ 0.26 (s, 9H), 2.19 (s, 6H), 2.32 (s, 3H), 6.06 (m, 2H), 6.11 (s, 1H), 6.68 (m, 2H), 6.93 (s, 2H), 7.49 (d, J = 7.8 Hz, 2H), 7.55 (d, J = 8.1 Hz, 2H), 7.63 (d, J = 8.1 Hz, 2H), 7.69 (d, J = 7.8 Hz, 2H), 10.43 (br s, 2H); ^{13}C NMR δ −0.2, 20.8, 39.2, 97.1, 104.3, 110.7, 121.2, 126.3, 129.2, 130.0, 130.3, 130.5, 130.8, 131.2, 131.4, 133.0, 136.9, 137.0, 137.4, 137.7, 140.3, 140.6, 182.4, 182.7. Anal. Calcd ($C_{37}H_{35}BrN_2O_2Si$): C, 68.61; H, 5.45; N, 4.33. Found: C, 68.88; H, 5.26; N, 4.08.

1,9-Bis(pentafluorobenzoyl)-5-(4-iodophenyl)dipyrromethane (5d). Following a general procedure,[20] a solution of **2b** (2.00 g, 5.74 mmol) in dry toluene (95 mL) was treated with EtMgBr (11.5 mL, 11.5 mmol, 1 M in THF) followed by a solution of pentafluorobenzoyl chloride (1.34 g, 5.81 mmol) in toluene (6 mL). Second and third additions (identical amounts; half the amounts, respectively) were performed after 10 and 20 min, followed by the standard workup. Column chromatography [silica, CH_2Cl_2–ethyl acetate (95 : 5)] afforded the crude diacyldipyrromethane, which was dissolved in CH_2Cl_2 and then precipitated with hexanes. Filtration and washing with hexanes afforded a fluffy white powder (1.70 g, 40%): mp 138–140 °C; ^{1}H NMR δ 5.60 (s, 1H), 6.12 (m, 2H), 6.67 (m, 2H), 6.97 (d, J = 8.1 Hz, 2H), 7.71 (d, J = 8.1 Hz, 2H), 9.80 (br s, 2H); ^{13}C NMR δ 44.5, 94.3, 112.9, 114.3, 123.6, 130.9, 132.2, 138.8, 139.9, 140.0, 142.9, 143.2, 146.3, 173.1. Anal. Calcd ($C_{29}H_{11}F_{10}IN_2O_2$): C, 47.31; H, 1.51; N, 3.80. Found: C, 47.49; H, 1.73; N, 3.64.

5-[4-(Hexyloxy)phenyl]-15-mesityl-10-(4-methoxyphenyl)-20-{4-[2-(trimethylsilyl)ethynyl]phenyl}porphyrin (6a). Following a general procedure,[20] a solution of diacyldipyrromethane **5a** (2.00 g, 3.34 mmol) in dry THF–methanol (10 : 1, 132 mL) was reduced with $NaBH_4$ (2.53 g, 66.8 mmol) affording the corresponding dipyrromethane-dicarbinol. The dipyrromethane-dicarbinol was condensed with dipyrromethane **2g** (1.08 g, 3.34 mmol) in acetonitrile (1.34 L) containing TFA (3.09 mL, 40.1 mmol). After 4 min, DDQ (2.27 g, 10.0 mmol) was added and the mixture was stirred at room temperature for 1 h. The standard workup afforded a purple solid (662 mg, 22%): ^{1}H NMR δ −2.70 (br s, 2H), 0.38 (s, 9H), 0.99 (t, 3H), 1.53 (m, 4H), 1.63 (m, 2H), 1.84 (s, 6H), 1.99 (m, 2H), 2.63 (s, 3H), 4.10 (s, 3H), 4.25 (t, 2H), 7.26–7.29 (m, 6H), 7.87 (d, J = 8.1 Hz, 2H), 8.09 (d, J = 9.0 Hz, 2H), 8.13 (d, J = 9.0 Hz, 2H), 8.17 (d, J = 8.1 Hz, 2H), 8.7–8.9 (m, 8 H); LD-MS obsd 881.6; HRMS (FAB) obsd 882.4367, calcd 882.4329 ($C_{59}H_{58}N_4O_2Si$); λ_{abs} 423, 517, 553, 594, 651 nm.

5-[4-(Hexyloxy)phenyl]-10-(4-iodophenyl)-15-mesityl-20-{4-[2-(trimethylsilyl)ethynyl]phenyl}porphyrin (6b). Reduction of **5c** (2.57 g, 3.70 mmol) followed by condensation with **2g** (1.19 g, 3.70 mmol) for 3 min, oxidation with DDQ (2.52 g, 11.1 mmol), and standard workup furnished a purple solid (790 mg, 22%): ^{1}H NMR δ −2.73 (br s, 2H), 0.38 (s, 9H), 1.00 (t, 3H), 1.47 (m, 4H), 1.65 (m, 2H), 1.84 (s, 6H), 1.99 (m, 2H), 2.64 (s, 3H), 4.26 (t, 2H), 7.29 (s, 4H), 7.87 (d, J = 8.1 Hz, 2H), 7.95 (d, J = 8.1 Hz, 2H), 8.09 (d, J = 7.8 Hz, 4H), 8.17 (d, J = 8.1 Hz, 2H), 8.7–8.9 (m, 8H); LD-MS obsd 979.8; HRMS (FAB) obsd 979.3278, calcd 979.3268 ($C_{58}H_{55}IN_4OSi$); λ_{abs} 422, 516, 552, 594, 651 nm.

5-(4-Bromophenyl)-10,20-dimesityl-15-{4-[2-(trimethylsilyl)-ethynyl]phenyl}porphyrin (6c). Reduction of **5b** (1.40 g, 2.16 mmol) followed by condensation with **2a** (0.57 g, 2.2 mmol) for 3 min, oxidation with DDQ (1.47 g, 6.47 mmol), and standard workup furnished a purple solid (484 mg, 26%): ^{1}H NMR δ −2.68 (br s, 2H), 0.37 (s, 9H), 1.83 (s, 12 H), 2.63 (s, 6H), 7.28 (s, 4H), 7.84–7.89 (m, 4H), 8.08 (d, J = 8.1 Hz, 2H), 8.16 (d, J = 8.1 Hz, 2H), 8.69–8.77 (m, 8H); LD-MS obsd 873.0; HRMS (FAB) obsd 872.2898, calcd, 872.2910 ($C_{55}H_{49}BrN_4Si$); λ_{abs} 420, 515, 549, 592, 649 nm.

5-(4-Iodophenyl)-10,20-dimesityl-15-{4-[2-(trimethylsilyl)-ethynyl]phenyl}porphyrin (6d). Reduction of **5c** (2.30 g, 3.31 mmol) followed by condensation with **2a** (0.87 g, 3.3 mmol) for 3 min, oxidation with DDQ (2.31 g, 9.93 mmol), and standard workup furnished a purple solid (0.66 g, 22%). The ^{1}H NMR and LD-MS data were identical to samples prepared by a mixed-aldehyde condensation.[51]

5-(4-Iodophenyl)-10,20-bis(pentafluorophenyl)-15-{4-[2-(trimethylsilyl)ethoxycarbonyl]phenyl}porphyrin (6e). Reduction of **5d** (2.21 g, 3.00 mmol) followed by condensation with **2f** (1.10 g, 3.00 mmol) for 5 min, oxidation with DDQ (2.04 g, 9.00 mmol), and standard workup furnished a purple solid. A second column [silica, CH_2Cl_2–hexanes (1:1)] yielded a purple solid (562 mg, 18%): ^{1}H NMR δ −2.89 (s, 2H), 0.18 (s, 9H), 1.30 (t, 2H), 4.62 (t, 2H), 7.95 (d, J = 8.7 Hz, 2H), 8.13 (d, J = 8.7 Hz, 2H), 8.30 (d, J = 8.7 Hz, 2H), 8.46 (d, J = 8.7 Hz, 2H), 8.8–9.0 (m, 8H); LD-MS obsd 1066.7; HRMS (FAB) obsd 1064.1105, calcd 1064.1101 ($C_{50}H_{31}F_{10}IN_4O_2Si$); λ_{abs} 419, 512, 545, 589, 644 nm.

5,15-Bis(pentafluorophenyl)-10-phenyl-20-{4-[2-(trimethylsilyl)-ethoxycarbonyl]phenyl}porphyrin (6f). Reduction of **5e** (134 mg, 0.22 mmol) followed by condensation with **2f** (80.6 mg, 0.22 mmol) for 7 min, oxidation with DDQ (150 mg, 0.66 mmol), and standard workup furnished a purple solid. A second column [silica, CH_2Cl_2–hexanes (1 : 1)] yielded a purple solid (39.2 mg, 19%): ^{1}H NMR (400 MHz) δ −2.86 (s, 2H), 0.18 (s, 9H), 1.30 (t, 2H), 4.62 (t, 2H), 7.78–7.82 (m, 3H) 8.21 (d, J = 8.0 Hz, 2H), 8.30 (d, J = 8.4 Hz, 2H), 8.46 (d, J = 7.2 Hz,

2H), 8.80–8.82 (m, 4H), 8.90 (d, J = 4.4 Hz, 2H), 8.95 (d, J = 4.4 Hz, 2H); LD-MS obsd 938.0; HRMS (FAB) obsd 1064.1105, calcd 1064.1101 ($C_{50}H_{32}F_{10}N_4O_2Si$); λ_{abs} 418, 512, 544, 589, 643 nm.

5-(4-Bromophenyl)-10,15,20-tri-*p*-tolylporphyrin (6g). Reduction of **5f** (0.54 g, 1.2 mmol) followed by condensation with **2c** (0.35 g, 1.2 mmol) for 3 min, oxidation with DDQ (0.79 g, 3.4 mmol), and standard workup furnished a purple solid (210 mg, 25%): ^{1}H NMR δ −2.79 (s, 2H), 2.71 (br s, 9H), 7.56 (d, J = 8.4 Hz, 6H), 7.89 (d, J = 9.0 Hz, 2H), 8.08–8.11 (m, 8H), 8.80 (d, J = 4.2 Hz, 2H), 8.87–8.90 (m, 6H); LD-MS obsd 734.3; HRMS (FAB) obsd 734.2083, calcd 734.2045 ($C_{47}H_{35}BrN_4$); λ_{abs} 421, 516, 551, 593, 648 nm.

Zinc(II)-5-[4-(Hexyloxy)phenyl]-15-mesityl-10-(4-methoxyphenyl)-20-{4-[2-(trimethylsilyl)ethynyl]phenyl}porphyrin (Zn-6a). To a solution of **6a** (147 mg, 0.166 mmol) in $CHCl_3$ (50 mL) was added a solution of $Zn(OAc)_2{\cdot}2H_2O$ (182 mg, 0.831 mmol) in methanol (6 mL). The reaction mixture was stirred at room temperature for 16 h. The reaction mixture was washed with water, dried (Na_2SO_4), and concentrated. Column chromatography (silica, CH_2Cl_2) afforded a purple solid (142 mg, 91%): ^{1}H NMR δ 0.38 (s, 9H), 1.00 (t, 3H), 1.49 (m, 4H), 1.64 (m, 2H), 1.83 (s, 6H), 2.00 (m, 2H), 2.64 (s, 3H), 4.09 (s, 3H), 4.26 (t, 2H), 7.29 (s, 6H), 7.87 (d, J = 8.1 Hz, 2H), 8.10 (d, J = 8.7 Hz, 2H), 8.14 (d, J = 8.7 Hz, 2H), 8.18 (d, J = 8.1 Hz, 2H), 8.8–9.0 (m, 8H); LD-MS obsd 942.7; HRMS (FAB) obsd 944.3470, calcd 944.3464 ($C_{59}H_{56}N_4O_2SiZn$); λ_{abs} 427, 552, 593 nm.

Zinc(II)-5-[4-(Hexyloxy)phenyl]-10-(4-iodophenyl)-15-mesityl-20-{4-[2-(trimethylsilyl)ethynyl]phenyl}porphyrin (Zn-6b). A sample of **6b** (160 mg, 0.163 mmol) was treated with $Zn(OAc)_2{\cdot}2H_2O$ (179 mg, 0.816 mmol) following the general procedure. Column chromatography (silica, CH_2Cl_2) afforded a purple solid (149 mg, 88%): ^{1}H NMR δ 0.38 (s, 9H), 1.00 (t, 3H), 1.48 (m, 4H), 1.65 (m, 2H), 1.83 (s, 6H), 1.99 (m, 2H), 2.64 (s, 3H), 4.26 (t, 2H), 7.29 (s, 4H), 7.87 (d, J = 8.1 Hz, 2H), 7.97 (d, J = 8.7 Hz, 2H), 8.10 (m, 4H), 8.18 (d, J = 8.1 Hz, 2H), 8.8–9.0 (m, 8H); LD-MS obsd 1040.7; HRMS (FAB) obsd 1040.2318, calcd 1040.2325 ($C_{58}H_{53}IN_4OSiZn$); λ_{abs} 427, 552, 594 nm.

Zinc(II)-5-(4-Bromophenyl)-10,20-dimesityl-15-{4-[2-(trimethylsilyl)-ethynyl]phenyl}porphyrin (Zn-6c). A sample of **6c** (262 mg, 300 μmol) was treated with $Zn(OAc)_2{\cdot}2H_2O$ (329 mg, 1.50 mmol) following the general procedure. Column chromatography [silica, $CHCl_3$–hexanes (7 : 3)] afforded a purple solid (265 mg, 94%). ^{1}H NMR δ 0.37 (s, 9H), 1.82 (s, 12H), 2.63 (s, 6H), 7.28 (s, 4H), 7.84–7.89 (m, 4H), 8.10 (d, J = 8.1 Hz, 2H), 8.18 (d, J = 8.7 Hz, 2H), 8.77–8.79 (m, 4H), 8.84–8.86 (m, 4H); LD-MS obsd 936.5; HRMS (FAB) obsd 934.2055, calcd 934.2045 ($C_{55}H_{47}BrN_4SiZn$); λ_{abs} 419, 550, 590 nm.

Zinc(II)-5-(4-Iodophenyl)-10,20-dimesityl-15-{4-[2-(trimethylsilyl)ethynyl]phenyl}porphyrin (Zn-6d). A sample of **6d** (0.38 g, 0.41 mmol) was treated with $Zn(OAc)_2{\cdot}2H_2O$ (0.45 g, 2.1 mmol) following the general procedure. Purification was achieved by suspension in methanol, followed by filtration to afford a purple solid (0.36 g, 90%): ^{1}H NMR δ 0.37 (s, 9H), 1.82 (s, 12H), 2.63 (s, 6H), 7.28 (s, 4H), 7.86 (d, J = 8.1 Hz, 2H), 7.97 (d, J = 8.1 Hz, 2H), 8.08 (d, J = 8.1 Hz, 2H), 8.18 (d, J = 7.8 Hz, 2H), 8.77–8.79 (m, 4H), 8.84–8.87 (m, 4H); LD-MS obsd 983.1; HRMS (FAB) obsd 982.1943, calcd 982.1906 ($C_{55}H_{47}IN_4SiZn$); λ_{abs} 425, 550, 592 nm.

Magnesium(II)-5-(4-Iodophenyl)-10,20-bis(pentafluorophenyl)-15-{4-[2-(trimethylsilyl)ethoxycarbonyl]phenyl}porphyrin (Mg-6e). Following a general procedure,[22] a solution of **6e** (106 mg, 99.4 μmol) in CH_2Cl_2 (15 mL) was treated with TEA (690 μL, 4.92 mmol) followed by $MgBr_2{\cdot}O(Et)_2$ (639 mg, 2.47 mmol). After 30 min, the mixture was diluted with CH_2Cl_2 (20 mL), washed with 5% $NaHCO_3$, dried (Na_2SO_4), and concentrated. Column chromatography (alumina, CH_2Cl_2) afforded a purple solid (83 mg, 77%): ^{1}H NMR (THF-d_8) δ 0.20 (s, 9H), 1.31 (t, 2H), 4.61 (t, 2H), 7.98 (d, J = 8.1 Hz, 2H), 8.14 (d, J = 8.1 Hz, 2H), 8.31 (d, J = 8.1 Hz, 2H), 8.42 (d, J = 8.1 Hz, 2H), 8.80–8.90 (m, 8H); LD-MS obsd 1085.0; HRMS (FAB) obsd 1086.077, calcd 1086.079 ($C_{50}H_{29}F_{10}IMgN_4O_2Si$); λ_{abs} 427, 522, 561, 604 nm.

Magnesium(II)-5,15-Bis(pentafluorophenyl)-10-phenyl-20-{4-[2-(trimethylsilyl)ethoxycarbonyl]phenyl}porphyrin (Mg-6f). Following a general procedure,[22] a solution of **6f** (16.0 mg, 17.0 μmol) in CH_2Cl_2 (5 mL) was treated with TEA (94 μL, 0.68 mmol) followed by $MgBr_2{\cdot}O(Et)_2$ (88.0 mg, 0.34 mmol). The mixture was stirred at room temperature for 15 h. Column chromatography (silica, $CHCl_3$) afforded a purple solid (14.4 mg, 88%): ^{1}H NMR (400 MHz) δ 0.00 (s, 9H), 0.79 (t, 2H), 3.40 (br s, 2H), 7.75–7.79 (m, 5H), 8.03 (d, J = 8.4 Hz, 2H), 8.23 (d, J = 6.8 Hz, 2H), 8.76 (d, J = 4.8 Hz, 2H), 8.81–8.84 (m, 4H), 8.98 (d, J = 4.4 Hz, 2H); LD-MS obsd 958.4; HRMS (FAB) obsd 960.1891, calcd 960.1829 ($C_{50}H_{30}F_{10}MgN_4O_2Si$); λ_{abs} 426, 522, 561, 604 nm.

Zinc(II)-5-(4-Bromophenyl)-10,15,20-tri-*p*-tolylporphyrin (Zn-6g). A sample of **6g** (54 mg, 74 μmol) was treated with $Zn(OAc)_2{\cdot}2H_2O$ (80 mg, 0.36 mmol) following the general procedure. Column chromatography (silica, $CHCl_3$) afforded a purple solid (44 mg, 75%): ^{1}H NMR δ 2.72 (s, 9H), 7.56 (d, J = 7.2 Hz, 6H), 7.89 (d, J = 8.1 Hz, 2H), 8.11 (d, J = 7.5 Hz, 8H), 8.89–8.96 (m, 8H); LD-MS obsd 797.7; HRMS (FAB) obsd 796.1185, calcd 796.1180 ($C_{47}H_{33}BrN_4Zn$); λ_{abs} 424, 514, 551, 590 nm.

Magnesium(II)-5-(4-Bromophenyl)-10,15,20-tri-*p*-tolylporphyrin (Mg-6g). Following a general procedure,[22] a solution of **6g** (100 mg, 136 μmol) in CH_2Cl_2 (30 mL) was treated with *N,N*-diisopropylethylamine (1.18 mL, 6.80 mmol) and MgI_2 (1.89 g, 6.80 mmol). After 2 h, the mixture was washed with 5% $NaHCO_3$, dried (Na_2SO_4), and concentrated. Column chromatography (alumina, $CHCl_3$) afforded a purple solid (84 mg, 81%): ^{1}H NMR δ 2.72 (s, 9H), 7.54 (d, J = 7.2 Hz, 6H), 7.87 (d, J = 8.1 Hz, 2H), 8.09–8.12 (m, 8H), 8.82 (d, J = 5.1 Hz, 2H), 8.89–8.92 (m, 6H); LD-MS obsd 758.5; HRMS (FAB) obsd 756.1766, calcd 756.1739 ($C_{47}H_{33}BrMgN_4$); λ_{abs} 428, 526, 565, 605 nm.

Zinc(II)-5-(4-Ethynylphenyl)-10-[4-(hexyloxy)phenyl]-20-mesityl-15-(4-methoxyphenyl)porphyrin (Zn-6a′). A mixture of **Zn-6a** (138 mg, 0.146 mmol) and TBAF (175 μL, 175 μmol, 1.0 M in THF) in THF–$CHCl_3$ (12 mL, 2 : 1) was stirred at room temperature for 3 h. The solvent was removed and the residue was chromatographed (silica, CH_2Cl_2) yielding a purple solid (122 mg, 96%): ^{1}H NMR δ 0.99 (t, 3H), 1.47 (m, 4H), 1.64 (m, 2H), 1.84 (s, 6H), 1.99 (m, 2H), 2.64 (s, 3H), 3.31 (s, 1H), 4.09 (s, 3H), 4.26 (t, 2H), 7.26–7.29 (m, 4H), 7.88 (d, J = 8.1 Hz, 2H), 8.10 (d, J = 8.7 Hz, 2H), 8.14 (d, J = 8.7 Hz, 2H), 8.20 (d, J = 8.1 Hz, 2H), 8.70–8.90 (m, 10 H); LD-MS obsd 870.7; HRMS (FAB) obsd 872.3070, calcd 872.3069 ($C_{56}H_{48}N_4O_2Zn$); λ_{abs} 426, 552, 593 nm.

Zinc(II)-5-(4-Bromophenyl)-15-(4-ethynylphenyl)-10,20-dimesitylporphyrin (Zn-6c′). A mixture of **Zn-6c** (123 mg, 131 μmol) and TBAF (157 μL, 157 μmol, 1.0 M in THF) in THF–$CHCl_3$ (12 mL, 2 : 1) was stirred at room temperature for 30 min. The solvent was removed and the residue was chromatographed [silica, CH_2Cl_2–hexanes (7 : 3)] yielding a purple solid (87 mg, 77%): ^{1}H NMR δ 1.81 (s, 12H), 2.63 (s, 6H), 3.31 (s, 1H), 7.28 (s, 4H), 7.87 (d, J = 8.1 Hz, 4H), 8.10

(d, J = 8.1 Hz, 2H), 8.19 (d, J = 8.7 Hz, 2H), 8.78 (d, J = 6.0 Hz, 4H), 8.84 (d, J = 3.6 Hz, 4H); LD-MS obsd 859.1; HRMS (FAB) obsd 862.1624, calcd 862.1650 ($C_{52}H_{39}BrN_4Zn$); λ_{abs} 419, 550, 590 nm.

Dyad 9. To samples of **Zn-6g** (10 mg, 13 μmol), **Zn-6i′** (10 mg, 12 μmol), $Pd_2(dba)_3$ (2.1 mg, 2.3 μmol), and P(*o*-tol)$_3$ (4.8 mg, 16 μmol) was added a degassed solution of toluene–TEA (5 : 1, 6 mL). The mixture was placed in an oil bath at 80 °C. Aliquots were removed at 1 h and 3 h and analyzed by analytical SEC and LD-MS. The reaction mixture was passed over a silica column (THF), then loaded onto a preparative SEC column (THF). The dyad fraction was concentrated and analyzed by analytical SEC and LD-MS (with or without added POPOP, see text).

Dyad 10. To samples of **Mg-6g** (9.4 mg, 11.3 μmol), **Zn-6i′** (8.4 mg, 11.1 μmol), $Pd_2(dba)_3$ (1.6 mg, 1.7 μmol), and P(*o*-tol)$_3$ (3.7 mg, 12 μmol) was added a degassed solution of toluene–TEA (5 : 1, 6 mL). The reaction mixture was placed in an oil bath at 50 °C. Aliquots were removed at 1 h and 2 h timepoints for analysis (LD-MS and SEC, 1 h timepoint, SEC, 2 h timepoint). After 2 h, the reaction appeared to stop (based on SEC data); therefore, another batch of catalyst was added [1.8 mg $Pd_2(dba)_3$; 3.9 mg P(*o*-tol)$_3$]. After an additional 1 h, SEC analysis of a reaction aliquot indicated the reaction was complete. The mixture was filtered through a short alumina column ($CHCl_3$), chromatographed on SEC (THF) and filtered through a silica column ($CHCl_3$) affording a purple powder (12.6 mg, 75%): ^{1}H NMR δ 1.88 (s, 18H), 2.65 (s, 9H), 2.73 (s, 9H), 7.28–7.30 (m, 6H), 7.55–7.58 (m, 6H), 8.06 (d, J = 8.1 Hz, 4H), 8.12–8.15 (m, 6H), 8.30–8.33 (m, 4H), 8.72 (s, 4H), 8.80 (d, J = 4.2 Hz, 2H), 8.91–8.96 (m, 10H); LD-MS obsd 1503.2; FAB-MS obsd 1505.555, calcd 1505.549 ($C_{102}H_{78}MgN_8Zn$); λ_{abs} 431, 553, 564, 606 nm.

Dyad 11′. Following a general procedure,[25] **Zn-6a′** (54.1 mg, 61.9 μmol) and **Zn-6b** (62.5 mg, 60.0 μmol) were coupled using $Pd_2(dba)_3$ (11.7 mg, 12.8 μmol) and P(*o*-tol)$_3$ (22.7 mg, 74.5 μmol) in toluene–TEA (20 mL, 5 : 1) at 35 °C for 3 h. Concentration of the mixture afforded a purple–brown solid. The solid was filtered [silica, 4 × 8 cm, hexanes–CH_2Cl_2 (1 : 1)] to remove P(*o*-tol)$_3$, and the porphyrinic products were eluted (CH_2Cl_2). After a preparative SEC column (THF), the dyad fraction was concentrated, dissolved in $CHCl_3$, and chromatographed [silica, 4 × 8 cm, $CHCl_3$–hexanes (4 : 1)], yielding a purple solid (61 mg, 57%): ^{1}H NMR δ 0.38 (s, 9H), 1.00 (t, 6H), 1.48 (m, 8H), 1.65 (m, 4H), 1.87 (s, 12H), 2.00 (m, 4H), 2.65 (s, 6H), 4.10 (s, 3H), 4.27 (t, 4H), 7.26–7.31 (m, 8H), 7.90 (d, J = 8.1 Hz, 2H), 8.06–8.23 (m, 14H), 8.32 (d, J = 7.2 Hz, 4H), 8.80–9.06 (m, 16H); LD-MS obsd 1783.8; HRMS (FAB) obsd 1788.63, calcd 1788.63 ($C_{114}H_{100}N_8O_3SiZn_2$); λ_{abs} 430, 516, 552, 593 nm.

A solution of the porphyrin (61 mg, 34 μmol) in THF–$CHCl_3$ (8 mL, 2 : 1) was treated with TBAF (40 μL, 40 μmol, 1.0 M in THF). The mixture was stirred at room temperature for 2 h. The solvent was removed and the sample was redissolved in $CHCl_3$ (20 mL). The solution was washed with 10% aqueous $NaHCO_3$ (20 mL) and water. The organic layer was dried (Na_2SO_4), filtered, and concentrated. Purification by column chromatography [silica, 4 × 10 cm, $CHCl_3$–hexanes (4 : 1)] afforded a purple solid (53 mg, 91%): ^{1}H NMR δ 1.00 (t, 6H), 1.48 (m, 8H), 1.65 (m, 4H), 1.87 (s, 12H), 2.00 (m, 4H), 2.65 (s, 6H), 3.32 (s, 1H), 4.10 (s, 3H), 4.27 (t, 4H), 7.26–7.31 (m, 8H), 7.90 (d, J = 8.1 Hz, 2H), 8.06–8.23 (m, 14H), 8.32 (d, J = 7.2 Hz, 4H), 8.80–9.06 (m, 16H); LD-MS obsd 1710.7; HRMS (FAB) obsd 1712.58, calcd 1712.59 ($C_{111}H_{92}N_8O_3Zn_2$); λ_{abs} 430, 516, 553, 594 nm.

Triad 12. Samples of **11′** (35.5 mg, 20.7 μmol) and **Mg-6e** (26.1 mg, 24.0 μmol) were coupled with $Pd_2(dba)_3$ (5.2 mg, 5.7 μmol) and P(*o*-tol)$_3$ (8.9 mg, 29 μmol) in toluene–TEA (5 : 1, 7.0 mL) at 35 °C for 2 h. The volatile components were removed and the solid was filtered through an alumina column ($CHCl_3$–hexanes, 4 : 1). Porphyrin-containing fractions were concentrated and the mixture was chromatographed (SEC, THF). Column chromatography [alumina, $CHCl_3$–hexanes (4 : 1) followed by slow enrichment with THF] afforded a purple solid (41.2 mg, 75%): ^{1}H NMR (500 MHz) (THF-d_8) δ 0.17 (s, 9H), 0.99 (m, 6H), 1.28 (t, 2H), 1.60–1.75 (m, 8H), 1.80-1.90 (m, 4H), 1.85 (s, 6H), 1.88 (s, 6H), 1.97 (m, 4H), 2.59 (s, 3H), 2.61 (s, 3H), 4.04 (s, 3H), 4.26 (m, 4H), 4.59 (t, 2H), 7.26–7.31 (m, 12H), 8.04–8.11 (m, 12H), 8.28–8.32 (m, 8H), 8.40 (d, J = 7.8 Hz, 4H), 8.65 (d, J = 4.5 Hz, 2H), 8.71 (d, J = 4.5 Hz, 2H), 8.74 (d, J = 4.5 Hz, 4H), 8.81–8.95 (m, 16H); MALDI-MS obsd 2676.2, calcd avg mass 2675.9 ($C_{161}H_{120}F_{10}MgN_{12}O_5SiZn_2$); λ_{abs} 427, 435, 521, 558, 599 nm.

Triad 12′. To a sample of **12** (15 mg, 5.6 μmol) in THF–DMF (4 mL, 1 : 1) was added TBAF (6.7 μL, 6.7 μmol, 1.0 M in THF). The mixture was stirred at room temperature until LD-MS showed no starting material (24 h). Additional THF (5 mL) was added and the solution was poured into 50 mL of water. The resulting solid was filtered, washed copiously with water and then with methanol, yielding a purple solid (10.4 mg, 72%): LD-MS obsd 2571.46, calcd avg mass 2575.9 ($C_{156}H_{108}F_{10}MgN_{12}O_5Zn_2$); λ_{abs} 427, 435, 520, 561, 602 nm.

Dyad 13. Samples of **Zn-6c′** (90.0 mg, 104 μmol) and **Mg-6e** (113.1 mg, 104 μmol) were coupled with $Pd_2(dba)_3$ (14.3 mg, 15.6 μmol) and P(*o*-tol)$_3$ (38.0 mg, 125 μmol) in toluene–TEA (5 : 1, 40 mL). The mixture was stirred at room temperature for 105 min, at which time additional $Pd_2(dba)_3$ (14.3 mg, 15.6 μmol) and P(*o*-tol)$_3$ (38.0 mg, 125 μmol) were added. After a total of 4 h 20 min, the reaction mixture was concentrated, then loaded onto an alumina column ($CHCl_3$). The resulting porphyrin-containing fractions were then loaded onto a preparative SEC column (THF). The nearly pure dyad fraction was then loaded onto a silica column [$CHCl_3$–hexanes–TEA (95 : 5 : 1)]. Trituration with hexanes followed by filtration afforded a purple solid (115 mg, 60%): ^{1}H NMR (THF-d_8) δ 0.20 (s, 9H), 1.31 (t, 2H), 1.86 (s, 12H), 2.62 (s, 6H), 4.61 (t, 2H), 7.32 (s, 4H), 7.91 (d, J = 9.0 Hz, 2H), 8.05–8.14 (m, 6H), 8.31 (dd, J^1 = 2.1 Hz, J^2 = 1.5 Hz, 6H), 8.42 (d, J = 7.8 Hz, 2H), 8.69 (d, J = 4.2 Hz, 2H), 8.72 (d, J = 4.2 Hz, 2H), 8.78 (d, J = 4.5 Hz, 2H), 8.83 (d, J = 5.1 Hz, 2H), 8.88–8.97 (m, 8H); LD-MS obsd 1824.7, calcd avg mass 1824.3 ($C_{102}H_{67}BrF_{10}MgN_8O_2SiZn$); λ_{abs} 430, 554, 591 nm.

Tetrad 14. Samples of **11′** (50.0 mg, 29.1 μmol) and **13** (53.1 mg, 29.1 μmol) were coupled using $Pd_2(dba)_3$ (4.0 mg, 4.4 μmol) and P(*o*-tol)$_3$ (10.6 mg, 34.9 μmol) in toluene–TEA (5 : 1, 18 mL) at 50 °C for 2.5 h. Then additional $Pd_2(dba)_3$ (4.0 mg, 4.4 μmol) and P(*o*-tol)$_3$ (10.6 mg, 34.9 μmol) were added. After a total of 5 h, the reaction mixture was concentrated, then chromatographed on alumina [toluene–THF (9 : 1)]. The porphyrin-containing fractions were then loaded onto a preparative SEC column (THF). Some streaking occurred during purification. A second SEC column was run (THF). The tetrad-containing fractions were passed over an alumina column [toluene–THF (9 : 1)] to afford a purple solid (43 mg, 43%): ^{1}H NMR (THF-d_8) δ 0.22 (s, 9H), 1.01 (m, 6H), 1.83 (s, 8H), 1.88 (s, 16H), 2.63 (s, 4H), 2.65 (s, 8H), remaining aliphatic CH_2 resonances are broad and cannot be integrated with accuracy, 4.07 (s, 3H), 4.24 (m, 4H), 6.91 (s, 8H), 7.34 (m, 12H), 8.10 (m, 16H), 8.34–8.42 (m, 12H), 8.75–8.97 (m, 32H); MALDI-MS obsd 3464.1, calcd avg mass 3460.2 ($C_{213}H_{158}F_{10}MgN_{16}O_5SiZn_3$); λ_{abs} 436, 551, 592 nm.

Tetrad 14′. To a solution of **14** (33.6 mg, 9.7 μmol) in THF–DMF (40 mL, 10 : 1) was added TBAF (14.6 μL, 14.6 μmol, 1.0 M in THF). The solution was stirred at 60 °C for 12 h. LD-MS still showed a significant amount of starting material; therefore another 15 μL of TBAF was added. The mixture was stirred for another 5 h (LD-MS did not detect any starting material). The mixture was concentrated to a purple solid and triturated with methanol. The suspension was filtered, then washed with methanol, H_2O, then methanol again to recover 16.3 mg (50%) of a purple solid: MALDI-MS obsd 3362.1, calcd avg mass 3360.0 ($C_{208}H_{146}F_{10}MgN_{16}O_5Zn_3$); λ_{abs} 435, 553, 594 nm.

Dyad 15. Samples of **Zn-6c′** (52.5 mg, 60.6 μmol) and **Zn-6d** (59.7 mg, 60.6 μmol) were coupled using $Pd_2(dba)_3$ (8.3 mg, 9.1 μmol) and P(*o*-tol)$_3$ (22.1 mg, 72.7 μmol) in toluene–TEA (5 : 1, 20 mL) at room temperature. An aliquot was removed after 1 h and analyzed by SEC. Because of the modest conversion to dyad, another identical batch of $Pd_2(dba)_3$ and P(*o*-tol)$_3$ was added after 1.5 h. After an additional 2 h (3.5 h total reaction time), an aliquot was removed and analyzed by SEC. After 4 h, the mixture was concentrated and passed through an alumina column (toluene). The porphyrin-containing fractions were concentrated, then loaded onto a preparative SEC column (THF). The dyad fraction was then passed through a silica column [toluene–THF (95 : 5)]. The purple solid was triturated with hexanes, filtered, then washed with hexanes, methanol, and then hexanes again. The solid was then dissolved in THF and concentrated, affording a purple solid (62.1 mg, 60%): ^{1}H NMR (THF-d_8) δ 0.36 (s, 9H), 1.87 (s, 24H), 2.62 (s, 12H), 7.32 (s, 8H), 7.83 (d, J = 8.1 Hz, 2H), 7.91 (d, J = 8.1 Hz, 2H), 8.06 (d, J = 8.1 Hz, 4H), 8.12 (d, J = 8.1 Hz, 2H), 8.19 (d, J = 8.1 Hz, 2H), 8.31 (d, J = 8.1 Hz, 4H), 8.68–8.73 (m, 8H), 8.78–8.80 (m, 4H), 8.89 (d, J = 4.5 Hz, 4H); LD-MS calcd avg mass 1722.1, obsd 1722.1 ($C_{107}H_{85}BrN_8SiZn_2$); λ_{abs} 429, 513, 550, 591 nm.

Dyad 15′. A solution of dyad **15** (65 mg, 38 μmol) in THF (7 mL) was treated with TBAF (45 μL, 45 μmol, 1.0 M in THF) and the mixture was stirred at room temperature for 1 h. The solvent was removed by rotary evaporation. Column chromatography (silica, toluene) afforded a purple solid (52 mg, 84%): ^{1}H NMR δ (toluene-d_8, 400 MHz) 2.11 (s, 24H) 2.55 (s, 12H), 2.93 (s, 1H), 7.27 (s, 8H), 7.58 (d, J = 8.0 Hz, 2H), 7.72 (d, J = 7.6 Hz, 2H), 7.78 (d, J = 8.0 Hz, 2H), 7.94 (d, J = 8.4 Hz, 2H), 8.00 (d, J = 8.0 Hz, 4H), 8.12 (d, J = 7.8 Hz, 4H), 8.84 (d, J = 4.4 Hz, 2H), 8.86 (d, J = 4.4 Hz, 2H), 8.90 (d, J = 4.8 Hz, 2H), 8.92 (d, J = 4.8 Hz, 2H), 8.95 (d, J = 4.8 Hz, 4H), 9.02 (d, J = 4.4 Hz, 4H); LD-MS obsd 1651.2; calcd avg mass 1649.5 ($C_{104}H_{77}BrN_8Zn_2$); λ_{abs} 429, 513, 550, 591 nm.

Tetrad 16. Samples of **15** (16.6 mg, 9.69 μmol) and **11′** (16.7 mg, 9.70 μmol) were coupled using $Pd_2(dba)_3$ (1.3 mg, 1.4 μmol) and P(*o*-tol)$_3$ (3.5 mg, 12 μmol) in toluene–TEA (5 : 1, 6 mL) at 50 °C. The reaction mixture was not homogeneous. Analytical SEC after 1 h showed 23% conversion to tetrad. After 90 min, additional $Pd_2(dba)_3$ (1.3 mg, 1.4 μmol) and P(*o*-tol)$_3$ (3.5 mg, 12 μmol) were added. Analytical SEC after 4.5 h showed 51% conversion to tetrad. After 5 h, the reaction mixture was loaded onto an alumina column [toluene–THF (95 : 5)]. The porphyrin fractions were dissolved in THF–toluene (95 : 5), then loaded onto a preparative SEC column (THF). The tetrad fraction was triturated with hexanes. The mixture was filtered. The filtered material was washed with hexanes, methanol, and then hexanes again. The solid was then dissolved in THF and concentrated affording a purple solid (10.1 mg, 31%): ^{1}H NMR (THF-d_8) δ 0.36 (s, 9H), 0.91 (t, 6H), 1.50 (m 4H), 1.88 (d, 36H), 2.63 (d, 18H), remaining aliphatic CH_2 resonances are buried under the large THF signal and the mesityl resonances, 4.07 (s, 3H), 4.29 (m, 4H), 7.32 (m, 20H), 8.09 (m, 24H), 8.32 (m, 8H), 8.68–8.78 (m, 12H), 8.83–8.97 (m, 20H); LD-MS obsd 3355.9, calcd avg mass, 3357.48 ($C_{218}H_{176}N_{16}O_3SiZn_4$); λ_{abs} 427, 435, 513, 552, 593 nm.

Triad 17. Samples of **15′** (46.6 mg, 28.2 μmol) and **Mg-6e** (30.7 mg, 28.2 μmol) were coupled using $Pd_2(dba)_3$ (3.9 mg, 4.2 μmol) and P(*o*-tol)$_3$ (7.7 mg, 25 μmol) in toluene–TEA (5 : 1, 18 mL) at room temperature for 2 h. Then additional $Pd_2(dba)_3$ (4.0 mg, 4.4 μmol) and P(*o*-tol)$_3$ (7.7 mg, 25 μmol) were added. After a total of 4.5 h, the reaction mixture was concentrated and chromatographed on alumina [toluene–THF (9 : 1)]. The porphyrin-containing fractions were then loaded onto a preparative SEC column (THF). The triad-containing fractions were passed over an alumina column [toluene–THF (9 : 1)] to afford a purple solid (38 mg, 51%): ^{1}H NMR (THF-d_8) δ 0.21 (s, 9H), 1.32 (t, 2H), 1.88 (s, 12H), 1.91 (s, 12H), 2.63 (s, 6H), 2.65 (s, 6H), 4.63 (t, 2H), 7.33 (s, 4H), 7.35 (s, 4H), 7.91 (d, J = 8.1 Hz, 2H), 8.07–8.15 (m, 10H), 8.31–8.35 (m, 10H), 8.44 (d, J = 8.1 Hz, 2H), 8.70–8.77 (m, 8H), 8.80 (d, J = 4.2 Hz, 2H), 8.85 (d, J = 4.5 Hz, 2H), 8.89–8.99 (m, 12H), multiplet centered at 7.15 and singlet at 2.33 are due to toluene; LD-MS obsd 2621.5, calcd avg mass 2608.6 ($C_{154}H_{105}BrF_{10}MgN_{12}O_2SiZn_2$); λ_{abs} 435, 553, 594 nm.

Pentad 18. Samples of **17** (19.5 mg, 11.4 μmol) and **11′** (27.0 mg, 10.4 μmol) were coupled using $Pd_2(dba)_3$ (1.4 mg, 1.6 μmol) and P(*o*-tol)$_3$ (2.9 mg, 9.4 μmol) in toluene–TEA (5 : 1, 8.5 mL) at 50 °C. THF (2 mL) was added and the mixture became homogeneous. An aliquot was removed after 70 min and analyzed by SEC, which revealed 25% conversion to pentad. After 1.5 h, another identical batch of catalyst was added. After 3 h, SEC revealed 38% conversion to pentad. The reaction was stopped after 5 h and the mixture was poured without concentration over an alumina column [toluene–THF (8 : 2)]. Some purple material remained bound to the top of the column. The porphyrin-containing fractions were loaded onto a preparative SEC column (THF). Purification was hampered by severe streaking. Only a small fraction of pentad was recovered ($\sim$2 mg) and due to its very poor solubility, could not be completely analyzed for purity. LD-MS obsd 4249.8, calcd avg mass 4244.5 ($C_{265}H_{196}F_{10}MgN_{20}O_5SiZn_4$); λ_{abs} 436, 563, 593 nm.

Dyad 19. Samples of **Zn-6i′** (30.0 mg, 36.2 μmol) and **Mg-6f** (39.4 mg, 36.2 μmol) were coupled using $Pd_2(dba)_3$ (6.6 mg, 7.2 μmol) and P(*o*-tol)$_3$ (13.2 mg, 43.4 μmol) in toluene–TEA (5 : 1, 15 mL) at 35 °C for 2.5 h. The mixture was passed through an alumina column ($CHCl_3$). Preparative SEC (THF) followed by column chromatography [silica, toluene–THF (98 : 2)] afforded a purple solid. Trituration with hexanes afforded a purple solid (38.7 mg, 60%): ^{1}H NMR (400 MHz) δ 0.06 (s, 9H), 1.87 (s, 18H), 2.63 (s, 3H), 2.65 (s, 6H), 3.71 (br s, 2H), 7.27 (s, 2H), 7.30 (s, 4H), 7.54 (br s, 2H), 8.03–8.06 (m, 6H), 8.12 (d, J = 7.6 Hz, 2H), 8.30 (d, J = 7.6 Hz, 4H), 8.73 (s, 4H), 8.81–8.87 (m, 6H), 8.91 (d, J = 4.4 Hz, 2H), 8.94 (d, J = 4.4 Hz, 2H), 9.08 (d, J = 4.4 Hz, 2H); LD-MS obsd 1790.16, calcd avg mass 1787.53 ($C_{105}H_{74}F_{10}MgN_8O_2SiZn_4$); λ_{abs} 430, 554, 590, 604 nm.

Acknowledgement

This work was supported by the Division of Chemical Sciences, Office of Basic Energy Sciences, Office of Energy Research, U.S. Department of Energy. Mass spectra were obtained at the Mass Spectrometry Laboratory for Biotechnology at North Carolina State University. Partial funding for the Facility was obtained from the North Carolina Biotechnology Center and

the National Science Foundation. We thank Dr. Richard Wagner for providing samples of **Mg-6g**, **Mg-6h′**, and **Zn-6h′**.

References

1 "Porphyrinic pigments" are members of a family that includes the parent porphyrin, the hydroporphyrins (chlorophylls, bacteriochlorophylls, *etc.*), species with skeletal atom replacements and/or annulations (tetraazaporphyrin, tetrabenzporphyrin, phthalocyanine, naphthalocyanine, *etc.*), ring-contracted or ring-expanded systems (corrole, sapphyrin, *etc.*), and species derived by combination of these variations, incorporation of peripheral substituents, and complexation with metals.

2 *The Photosynthetic Bacteria*, Eds. R. K. Clayton and W. R. Sistrom, Plenum Press, New York, 1978.

3 (*a*) J. H. Schön, Ch. Kloc, E. Bucher and B. Batlogg, *Nature*, 2000, **403**, 408; (*b*) B. A. Parkinson and M. T. Spitler, *Electrochimica Acta*, 1992, **37**, 943; (*c*) D. Cahen, G. Hodes, M. Grätzel, J. F. Guillemoles and I. Riess, *J. Phys. Chem. B*, 2000, **104**, 2053; (*d*) W. J. Albery, *Acc. Chem. Res.*, 1982, **15**, 142.

4 J.-S. Hsiao, B. P. Krueger, R. W. Wagner, T. E. Johnson, J. K. Delaney, D. C. Mauzerall, G. R. Fleming, J. S. Lindsey, D. F. Bocian and R. J. Donohoe, *J. Am. Chem. Soc.*, 1996, **118**, 11181.

5 J. P. Strachan, S. Gentemann, J. Seth, W. A. Kalsbeck, J. S. Lindsey, D. Holten and D. F. Bocian, *J. Am. Chem. Soc.*, 1997, **119**, 11191.

6 S. I. Yang, R. K. Lammi, J. Seth, J. A. Riggs, T. Arai, D. Kim, D. F. Bocian, D. Holten and J. S. Lindsey, *J. Phys. Chem. B*, 1998, **102**, 9426.

7 J. Seth, V. Palaniappan, R. W. Wagner, T. E. Johnson, J. S. Lindsey and D. F. Bocian, *J. Am. Chem. Soc.*, 1996, **118**, 11194.

8 J. Seth, V. Palaniappan, T. E. Johnson, S. Prathapan, J. S. Lindsey and D. F. Bocian, *J. Am. Chem. Soc.*, 1994, **116**, 10578.

9 D. Holten, D. F. Bocian and J. S. Lindsey, *Acc. Chem. Res.*, 2002, **35**, 57.

10 (*a*) T. A. Moore, D. Gust, P. Mathis, J.-C. Mialocq, C. Chachaty, R. V. Bensasson, E. J. Land, D. Doizi, P. A. Liddell, W. R. Lehman, G. A. Nemeth and A. L. Moore, *Nature*, 1984, **307**, 630; (*b*) P. A. Liddell, D. Barrett, L. R. Makings, P. J. Pessiki, D. Gust and T. A. Moore, *J. Am. Chem. Soc.*, 1986, **108**, 5350; (*c*) D. Gust, T. A. Moore, L. R. Makings, P. A. Liddell, G. A. Nemeth and A. L. Moore, *J. Am. Chem. Soc.*, 1986, **108**, 8028.

11 M. R. Wasielewski, M. P. Niemczyk, W. A. Svec and E. B. Pewitt, *J. Am. Chem. Soc.*, 1985, **107**, 5562.

12 (*a*) D. Gust, T. A. Moore, A. L. Moore, S.-J. Lee, E. Bittersmann, D. K. Luttrull, A. A. Rehms, J. M. DeGraziano, X. C. Ma, F. Gao, R. E. Belford and T. T. Trier, *Science*, 1990, **248**, 199; (*b*) J. Rodriguez, C. Kirmaier, M. R. Johnson, R. A. Friesner, D. Holten and J. L. Sessler, *J. Am. Chem. Soc.*, 1991, **113**, 1652; (*c*) D. Gust, T. A. Moore, A. L. Moore, A. N. Macpherson, A. Lopez, J. M. DeGraziano, I. Gouni, E. Bittersmann, G. R. Seely, F. Gao, R. A. Nieman, X. C. Ma, L. J. Demanche, S.-C. Hung, D. K. Luttrull, S.-J. Lee and P. K. Kerrigan, *J. Am. Chem. Soc.*, 1993, **115**, 11141.

13 (*a*) A. Osuka, R.-P. Zhang, K. Maruyama, N. Mataga, Y. Tanaka and T. Okada, *Chem. Phys. Lett.*, 1993, **215**, 179; (*b*) A. Osuka, S. Nakajima, K. Maruyama, N. Mataga, T. Asahi, I. Yamazaki, Y. Nishimura, T. Ohno and K. Nozaki, *J. Am. Chem. Soc.*, 1993, **115**, 4577.

14 (*a*) C. Luo, D. M. Guldi, H. Imahori, K. Tamaki and Y. Sakata, *J. Am. Chem. Soc.*, 2000, **122**, 6535; (*b*) G. Kodis, P. A. Liddell, L. de la Garza, P. C. Clausen, J. S. Lindsey, A. L. Moore, T. A. Moore and D. Gust, *J. Phys. Chem. B*, 2002, **106**, 2036.

15 S. R. Greenfield, W. A. Svec, D. Gosztola and M. R. Wasielewski, *J. Am. Chem. Soc.*, 1996, **118**, 6767.

16 R. H. Felton, in *The Porphyrins*, ed. D. Dolphin, Academic Press, New York, 1978, **vol. 5**, pp. 53–126.

17 J.-H. Fuhrhop and D. Mauzerall, *J. Am. Chem. Soc.*, 1969, **91**, 4174.

18 S. I. Yang, J. Seth, J.-P. Strachan, S. Gentemann, D. Kim, D. Holten, J. S. Lindsey and D. F. Bocian, *J. Porphyrins Phthalocyanines*, 1999, **3**, 117.

19 (*a*) R. K. Lammi, A. Ambroise, T. Balasubramanian, R. W. Wagner, D. F. Bocian, D. Holten and J. S. Lindsey, *J. Am. Chem. Soc.*, 2000, **122**, 7579; (*b*) R. K. Lammi, R. W. Wagner, A. Ambroise, J. R. Diers, D. F. Bocian, D. Holten and J. S. Lindsey, *J. Phys. Chem. B*, 2001, **105**, 5341; (*c*) R. K. Lammi, A. Ambroise, R. W. Wagner, J. R. Diers, D. F. Bocian, D. Holten and J. S. Lindsey, *Chem. Phys. Lett.*, 2001, **341**, 35.

20 P. D. Rao, S. Dhanalekshmi, B. J. Littler and J. S. Lindsey, *J. Org. Chem.*, 2000, **65**, 7323.

21 B. J. Littler, M. A. Miller, C.-H. Hung, R. W. Wagner, D. F. O'Shea, P. D. Boyle and J. S. Lindsey, *J. Org. Chem.*, 1999, **64**, 1391.

22 J. S. Lindsey and J. N. Woodford, *Inorg. Chem.*, 1995, **34**, 1063.

23 W. M. Sharman and J. E. Van Lier, *J. Porphyrins Phthalocyanines*, 2000, **4**, 441.

24 The coupling of porphyrin building blocks requires reaction conditions for the Sonogashira reaction that are different in several regards from those typically employed for non-porphyrinic molecules: (1) mild conditions must be employed to avoid demetalation and transmetalation reactions of metalloporphyrins, and to avoid metalation of Fb porphyrins; (2) copper cannot be employed, at least in the presence of Fb porphyrins; (3) the limited solubility of porphyrins requires couplings to be performed at modest concentrations (0.01–0.001 M); and (4) the iodo-porphyrin and the ethynyl-porphyrin generally need to be employed in a 1 : 1 ratio given the value of both components and the necessity for chromatographic workup. Accordingly, the conditions we developed for coupling iodo-porphyrins and ethynyl-porphyrins employ tris(dibenzylideneacetone)dipalladium(0) [$Pd_2(dba)_3$] and tri-*o*-tolylphosphine [P(*o*-tol)$_3$] in toluene–triethylamine (TEA) (5 : 1) at 35 °C in the absence of copper cocatalysts with equimolar amounts (~2.5 mM each) of the two porphyrins.[25]

25 R. W. Wagner, Y. Ciringh, C. Clausen and J. S. Lindsey, *Chem. Mater.*, 1999, **11**, 2974.

26 R. W. Wagner, T. E. Johnson and J. S. Lindsey, *J. Am. Chem. Soc.*, 1996, **118**, 11166.

27 J. Zhang, J. S. Moore, Z. Xu and R. A. Aguirre, *J. Am. Chem. Soc.*, 1992, **114**, 2273.

28 (*a*) O. Mongin, A. Schuwey, M.-A. Vallot and A. Gossauer, *Tetrahedron Lett.*, 1999, **40**, 8347; (*b*) S. Rucareanu, O. Mongin, A. Schuwey, N. Hoyler, A. Gossauer, W. Amrein and H.-U. Hediger, *J. Org. Chem.*, 2001, **66**, 4973.

29 (*a*) O. Henze, D. Lentz and A. D. Schlüter, *Chem. Eur. J.*, 2000, **6**, 2362; (*b*) M. S. Wong and J.-F. Nicoud, *Tetrahedron Lett.*, 1994, **35**, 6113; (*c*) S. Höger, A.-D. Meckenstock and S. Müller, *Chem. Eur. J.*, 1998, **4**, 2423; (*d*) Y. Tobe, N. Utsumi, A. Nagano and K. Naemura, *Angew. Chem., Int. Ed.*, 1998, **37**, 1285.

30 The analytical SEC data are uncorrected.

31 Tetrad **16** was almost totally insoluble in CH_2Cl_2 and $CHCl_3$, only slightly soluble in toluene and moderately soluble in THF. The highest solubility was obtained with mixtures of toluene and THF. Slight heating was sometimes necessary to achieve full dissolution of **16**.

32 The $E_{1/2}$ value for the transmission element in the rod can be estimated as follows. The $E_{1/2}$ value for a Zn porphyrin with two mesityl and two diphenylethyne groups is 0.61 V.[7] Inspection of Table 1 shows that replacement of a hydrogen on a phenyl ring with a *p*-methoxy group lowers the potential by ~20 mV per *p*-methoxy group; whereas replacing three methyl groups on a phenyl ring with hydrogens raises the potential by ~10 mV. Accordingly, the **Zn-6b**-derived transmission element in a rod would be expected to have an $E_{1/2}$ value in the vicinity of ~0.60 V. This value is ~30 mV higher than that measured for the **Zn-6b** building block (Table 2).

33 M. del Rosario Benites, T. E. Johnson, S. Weghorn, L. Yu, P. D. Rao, J. R. Diers, S. I. Yang, C. Kirmaier, D. F. Bocian, D. Holten and J. S. Lindsey, *J. Mater. Chem.*, 2002, **12**, 65–80.

34 The rate constant (k_{ENT}) and quantum efficiency (Φ_{ENT}) of energy transfer (Zn*Mg → ZnMg*) in dyad **19** are calculated using the observed Zn* lifetime in the dyad and the value of 2.4 ns in monomeric Zn porphyrin reference compounds (Table 3) using standard equations.[5] In THF, the values are $k_{ENT} = (9\ ps)^{-1} - (2.4\ ns)^{-1} = (9\ ps)^{-1}$ and $\Phi_{ENT} = 1 - (9\ ps)/(2.4\ ns) > 0.99$. Similar calculations for energy flow to the Mg porphyrin in the triad and tetrad in THF give $k_{ENT} = (15\ ps)^{-1}$ and $\Phi_{ENT} > 0.99$ for triad **12** and $k_{ENT} = (30\ ps)^{-1}$ and $\Phi_{ENT} = 0.99$ for tetrad **14**.

35 F. Li, S. Gentemann, W. A. Kalsbeck, J. Seth, J. S. Lindsey, D. Holten and D. F. Bocian, *J. Mater. Chem.*, 1997, **7**, 1245.

36 Small changes in the emission properties of **Mg-6f** compared to **MgU** can be understood by a small effect on the natural radiative (fluorescence) rate constant k_f. This effect is evident from the small change in the oscillator strength of the Q(0,0) absorption and emission transitions compared to **MgU**, and can be traced to fluorination effects on the porphyrin orbital energies, as has been described for other halogenated porphyrin monomers.[18]

37 The more polar solvent MeCN can also coordinate to the central

metal. Such coordination causes a change in the porphyrin radiative rate constant k_f, as is seen in the changes in the oscillator strength of the Q(0,0) absorption and emission bands (relative to the nearly constant Q(1,0) absorption and Q(0,1) emission strengths). The change in k_f must be taken into account in assessment of the quantum yields and lifetimes in different solvents.

38 The efficiency of $ZnMg^* \rightarrow Zn^+Mg^-$ hole transfer (Φ_{HT}) in dyad **19** can be calculated using the emission yield and lifetime data in Table 3 and the standard equations.[39] In toluene, the hole-transfer yield is found to be $\Phi_{HT} = 1 - (6.0\ ns)/(8.3\ ns) = 0.28$ from the lifetimes and $\Phi_{HT} = 1 - 0.087/0.14 = 0.38$ from the emission yields, giving an average value of $\sim$0.35. The same analysis for **19** in MeCN gives $\Phi_{HT} = 1 - (2.6\ ns)/(7.6\ ns) = 0.66$ and $\Phi_{HT} = 1 - 0.061/0.13 = 0.53$ for an average value of 0.60. These hole-transfer yields along with the Mg* lifetimes give hole-transfer rate constants of $k_{HT} = 0.35/(8.3\ ns) = (24\ ns)^{-1}$ in toluene and $k_{HT} = 0.60/(7.6\ ns) = (13\ ns)^{-1}$ in MeCN.

39 S. Prathapan, S. I. Yang, M. A. Miller, D. F. Bocian, D. Holten and J. S. Lindsey, *J. Phys. Chem. B*, 2001, **105**, 8237.

40 As a point of reference, Mg* in **ZnMgU** (which contains only mesityl groups at the non-linking meso positions) does not decay to any measurable degree by charge transfer, indicating that the charge-separated states lie above the excited state;[41] furthermore, based on the redox potentials of these porphyrins (and related molecules depicted in Tables 1 and 2) it is clear that if excited-state charge transfer were to occur in **ZnMgU** and similar dyads (as in polar media due to lowering of the charge-separated state below that of Mg*) then Mg* would transfer instead an electron to the Zn porphyrin to form Zn^-Mg^+. This is the opposite direction of charge flow to that required for the desired rectification effect (in either the ground or excited state) in the light-harvesting rods.

41 P. Hascoat, S. I. Yang, R. K. Lammi, J. Alley, D. F. Bocian, J. S. Lindsey and D. Holten, *Inorg. Chem.*, 1999, **38**, 4849.

42 J. Rodriguez, C. Kirmaier and D. Holten, *J. Am. Chem. Soc.*, 1989, **111**, 6500.

43 In the triad **12** and tetrad **14**, a faster component with a time constant of 2–3 ps is often seen in the kinetic data. This component includes energy transfer between Zn porphyrins and Zn*Zn* annihilation between adjacent units if more than one photon is absorbed in a given array. This latter effect is eliminated at very low excitation intensities, as we have found recently in studies of porphyrins containing 8 or 20 Zn porphyrins around a single Fb porphyrin in a dendrimeric architecture.[33]

44 S. I. Yang, J. Li, H. S. Cho, D. Kim, D. F. Bocian, D. Holten and J. S. Lindsey, *J. Mater. Chem.*, 2000, **10**, 283.

45 P. G. Seybold and M. Gouterman, *J. Mol. Spectrosc.*, 1969, **31**, 1.

46 P. D. Rao, B. J. Littler, G. R. Geier III and J. S. Lindsey, *J. Org. Chem.*, 2000, **65**, 1084.

47 D. Gryko and J. S. Lindsey, *J. Org. Chem.*, 2000, **65**, 2249.

48 J. Li, A. Ambroise, S. I. Yang, J. R. Diers, J. Seth, C. R. Wack, D. F. Bocian, D. Holten and J. S. Lindsey, *J. Am. Chem. Soc.*, 1999, **121**, 8927.

49 C.-H. Lee and J. S. Lindsey, *Tetrahedron*, 1994, **50**, 11427.

50 N. Nishino, R. W. Wagner and J. S. Lindsey, *J. Org. Chem.*, 1996, **61**, 7534.

51 M. Ravikanth, J.-P. Strachan, F. Li and J. S. Lindsey *Tetrahedron*, 1998, **54**, 7721.